A&A 496, 701–712 (2009)
DOI: 10.1051/0004-6361/200811070

Astronomy & Astrophysics

Abundances in bulge stars from high-resolution, near-IR spectra

I. The CNO elements observed during the science verification of CRIRES at VLT⋆,⋆⋆

N. Ryde[1,2], B. Edvardsson[2], B. Gustafsson[2], K. Eriksson[2], H. U. Käufl[3], R. Siebenmorgen[3], and A. Smette[4]

[1] Lund Observatory, Box 43, 22100 Lund, Sweden
e-mail: ryde@astro.lu.se
[2] Department of Astronomy and Space Physics, Uppsala University, Box 515, 75120 Uppsala, Sweden
[3] ESO, Karl-Schwarzschild-Str. 2, 85748 Garching, Germany
[4] ESO, Alonso de Cordova 3107, Vitacura, Casilla 19001, Santiago 19, Chile

Received 1 October 2008 / Accepted 11 January 2009

ABSTRACT

Context. The formation and evolution of the Milky Way bulge is not yet well understood and its classification is ambiguous. Constraints can, however, be obtained by studying the abundances of key elements in bulge stars.
Aims. The aim of this study is to determine the chemical evolution of C, N, O, and a few other elements in stars in the Galactic bulge, and to discuss the sensitivities of the derived abundances from molecular lines.
Methods. High-resolution, near-infrared spectra in the *H* band were recorded using the CRIRES spectrometer on the *Very Large Telescope*. Due to the high and variable visual extinction in the line-of-sight towards the bulge, an analysis in the near-IR is preferred. The C, N, and O abundances can all be determined simultaneously from the numerous molecular lines in the wavelength range observed.
Results. The three giant stars in Baade's window presented here are the first bulge stars observed with CRIRES during its *science verification observations*. We have especially determined the C, N, and O abundances, with uncertainties of less than 0.20 dex, from CO, CN, and OH lines. Since the systematic uncertainties in the derived C, N, and O abundances due to uncertainties in the stellar fundamental parameters, notably $T_{\rm eff}$, are significant, a detailed discussion of the sensitivities of the derived abundances is included. We find good agreement between near-IR and optically determined O, Ti, Fe, and Si abundances. Two of our stars show a solar [C+N/Fe], suggesting that these giants have experienced the first dredge-up and that the oxygen abundance should reflect the original abundance of the giants. The two giants fit into the picture, in which there is no significant difference between the oxygen abundance in bulge and thick-disk stars. Our determination of the sulphur abundances is the first for bulge stars. The high [S/Fe] values for all the stars indicate a high star-formation rate in an early phase of the bulge evolution.

Key words. stars: abundances – Galaxy: bulge – infrared: stars

1. Introduction

The origin and chemical properties of the Galactic bulge are poorly understood, see, for instance, the reviews by Wyse et al. (1997) and Kormendy & Kennicutt (2004). These properties are critical for our understanding of the formation and evolution of the Milky Way, but also of galaxies in general (Renzini 2006).

The classification of the Galactic bulge is also ambiguous: its structure and shape, with a peanut-formed profile and a small bar, dynamic and transient in nature, show signatures of the secularly evolved "pseudo-bulges". Binney (Ref. IAU254, in press) defines it as a clear case of a pseudo-bulge. These are typical for late-type galaxies, containing young stars, and believed to form slowly out of disk gas and stars (Kormendy & Kennicutt 2004).

However, the stars in the bulge seem to show ages and enhancements of α elements[1] relative to iron sooner characteristic of "classical bulges", suggesting that the star-formation period was early and very short (Lecureur et al. 2007; Fulbright et al. 2007). The classical bulges are typical for Sa and Sb galaxies, they are similar to elliptical galaxies, and are interpreted as formed through hierarchical clustering and merging events. Furthermore, they probably had most of their star formation long ago and therefore contain mostly old stars. Indeed, colour−magnitude diagrams indicate that most of the Galactic bulge stars formed more than 10 Gyr ago (Ortolani et al. 1995) and Zoccali et al. (2003) find no trace of a younger population in the bulge. Hence, the bulk of the bulge's stellar population is thought not to have formed by slow secular evolution. For instance, Minniti & Zoccali (2008) conclude in their review on the Galactic bulge, that a secular evolution of the disk forming a bulge can be excluded[2].

Hence, the formation of the Milky Way bulge is not well understood and its classification is still inconclusive. Since the different formation scenarios can be constrained by abundance

⋆ Based on observations collected at the European Southern Observatory, Chile (ESO Programme 60.A-9058A).
⋆⋆ Table 7 is only available in electronic from at http://www.aanda.org
[1] The α elements include O, Mg, Si, S, Ca, and Ti.
[2] Although there is a considerable agreement that there exists a dominant, old, metal-rich population in the bulge, there is some evidence of ongoing star formation and a younger population within of the order of 100 pc of the geometrical centre, see e.g. Figer et al. (2004) and Barbuy (2002).

surveys, more of them need to be performed. The two types of bulges give different dynamic and chemical signatures. From the α-element compositions relative to iron as a function of the metallicities, [Fe/H], of the stars, one can infer star-formation rates (SFR) and initial-mass functions (IMF) (see, for example, McWilliam & Rich 2004). A shallower IMF will increase the number of α-element producing stars thus leading to higher [α/Fe] values. A faster enrichment due to a high star-formation rate will keep the over-abundance of the α elements relative to iron at a high value also at higher metallicity. Different populations may show different behaviours.

To fully clarify the situation, a determination of the degree of mixing-in of other populations than the dominant one needs to be done. A search for other populations should be performed in different parts of the bulge, especially in the centre and along the galactic plane, by abundance surveys of bulge stars. Until now, the bulge has remained fairly unexplored, mainly because of the high and variable optical obscuration due to dust in the line-of-sight toward the Galactic centre. Other difficulties that affect investigations of bulge stars are the crowding of stars and the confusion of foreground stars. However, the infrared, with lower extinction ($A_K \sim 0.1 \times A_V$; Cardelli et al. 1989) and predominantly molecular rather than atomic abundance indicators, is a preferred wavelength region to study abundances in bulge stars (Ryde et al. 2005). This will allow the investigation of the entire bulge and not only regions with low optical obscuration. Discussions of abundances based on high-resolution spectroscopy in the IR are becoming more common due to spectrometers such as the Phoenix (Hinkle et al. 1998, 2003) and CRIRES spectrometers (Moorwood 2005; Käufl et al. 2006). In this paper, which is the first in a series, we have studied abundances in the first three bulge giants based on near-IR spectra observed with the CRIRES spectrometer, during its science Verification observations. We have in particular studied the abundances of the C, N, and O elements, as derived from molecular lines, and discuss their uncertainties.

2. Abundance determinations: going to the near-IR

In the wavelength range recorded by CRIRES, we have identified lines from which abundances can be derived for C, N, O, the α elements Si, S, Ti, and the iron peak elements Cr, Fe, and Ni. In particular, the abundances of the important C, N, and O elements can be better determined from a wealth of molecular lines in the near-IR, than in the optical. Apart from the fact that the extinction towards the bulge is lower at infrared wavelengths, there are other advantages of going to the near-IR.

2.1. Advantages and drawbacks of going to the near-IR

1. Red stars stand out the most in the near-IR not only because they are brightest there. Admittedly, the dust extinction decreases monotonically with wavelength, which favours longer wavelengths, but interstellar dust radiates strongly in the mid- and far-IR, and therefore the near-IR should be preferred. Furthermore, in the thermal infrared (i.e. beyond approximately 2.3 μm) the telluric sky and the telescope shine due to their intrinsic temperatures, making observations increasingly difficult, the longer the wavelength. Thus, this leaves us with the J, H, and K bands for an optimal spectroscopic study.
2. The near-IR is also preferred to the visual wavelength region for analysis of abundances due to the fact that the absorption spectra are less crowded with lines, that fewer lines are blended, and that it is easier to find portions of the spectrum which can be used to define a continuum. These are important facts which reduce the uncertainties in the derived abundances.
3. For the rotation-vibration bands in the IR that occur within the electronic gound state, the assumption of *local thermodynamic equilibrium (LTE)* in the analysis of the molecules is probably valid (Hinkle & Lambert 1975), which simplifies the correct analysis dramatically.
4. Moreover, in the Rayleigh-Jeans regime, the continuum intensity is less sensitive to temperature variations. This means that the effects of, for example, effective-temperature uncertainties or surface inhomogeneities on line strengths should be smaller in the IR[3].
5. Not least, it is important to realise that in general the determination of the oxygen abundance can only be carried out with confidence if the carbon abundance is well known, since the CO molecule holds most of the C and much of O in cool star atmospheres. Only the IR offers, even within a small wavelength range, all indicators necessary to accurately determine the C-N-O molecular and atomic equilibrium in the atmospheres of cool stars, through the simultaneous observation of many clean CO, CN and OH lines.

A general drawback of a spectral analysis in the near-IR is that there are much fewer atomic and ionic lines. The ones that exist often originate from highly excited levels in metal atoms, which also complicates an interpretation. Furthermore, many lines are not properly identified and/or lack known oscillator strengths, which are needed in an abundance analysis. Furthermore, even though great advances have been made in the technology for recording near-infrared light, existing spectrometers are still much less effective than optical ones, one of the main reasons being the lack of cross-dispersion. Finally, determining the stellar parameters based only on near-IR spectra is difficult.

Nevertheless, the near-IR is the optimal spectroscopic region to work in, in order to get a handle on the Milky Way bulge through abundance analysis. Recently, a few studies of elemental abundances of bulge stars using near-IR spectra at high resolution ($R \sim 50\,000$) have been performed with the Phoenix spectrometer, see for instance Meléndez et al. (2003), Cunha & Smith (2006), Cunha et al. (2007), and Meléndez et al. (2008). Interesting investigations of bulge stars have also been performed with NIRSPEC at the Keck II telescope at 1.5−1.8 μm, see for instance Origlia et al. (2002); Origlia & Rich (2003, 2004); Rich & Origlia (2005); Rich et al. (2007). However, in these studies, the spectral resolution is lower, $R \sim 25\,000$, which does not allow stellar lines to be fully resolved.

3. Observations

In the project "CNO abundances in bulge giants", we were granted 3 hours of science verification observations with CRIRES. CRIRES is a cryogenic echelle spectrograph designed for high spectral resolution, near-infrared observations. This paper is based on the spectra obtained during those observations, which were performed on 12 August 2006. Adaptive optics (MACAO – Multi-Applications Curvature Adaptive Optics) was used, which enhances the signal-to-noise ratio and the spatial resolution. The stars observed are Arp 4329, Arp 4203, and

[3] Note, however, that this effect also weakens the lines correspondingly.

Arp 1322[4] in Baade's Window. These stars were chosen among the bulge giants observed optically by Fulbright et al. (2006). The H magnitudes and the total exposure times, $t_{\rm exp}$, for each programme star are given in Table 1.

The slit width was 0.4″ yielding a spectral resolution of $R = \lambda/\Delta\lambda = 50\,000$ with four pixels per spectral resolution element. The wavelength range expected was 1532.6–1570.5 nm (in order 36) over the detector arrays, consisting of a mosaic of four Aladdin III InSb arrays in the focal plane. However, both the first and fourth detector arrays had problems[5]. Thus, only the spectra from the second and third arrays have been used for the analysis. Data for the first and fourth ones were used to confirm abundances when possible. This is, nevertheless, an improvement in wavelength coverage compared with the Phoenix detector, which corresponds to circa one of CRIRES's detector arrays ($\Delta\lambda = 0.5\%$). The approximate signal-to-noise ratios (*SNR*) per pixel-element in the dispersion direction (the spectrum collapsed in the spatial direction) at the continuum at 1554.8 nm of the observed spectra (in the third detector array), are also given in Table 1. The *SNR* per wavelength resolution element is a factor of 2 larger. The *SNR* varies by a factor of two between the detector arrays. The *SNR* of the second array varies approximately from 70% to 100% linearly with wavelength, whereas the third detector array, which is the best one, provides a relatively constant *SNR*.

The observed data were processed with standard routines in the reduction package `IRAF` (Tody 1993)[6], in order to retrieve one-dimensional, continuum normalised, and wavelength calibrated stellar spectra. The four arrays were reduced separately, resulting in four spectra, one for each array. In order to remove the detector dark current and the background emission from the thermal sky and telescope from the stellar frames, the telescope was nodded along the slit between the source and a region of the sky (in an "AB" configuration with a nod throw of 10″). The two equally long exposures were subtracted from each other, yielding two sky-subtracted exposures of the star. The reduced spectra from these exposures, were combined in `IRAF` with task `scombine`. In the wavelength region observed, the sky is relatively free from telluric lines, so no division by a standard star was made. The wavelength calibration was performed using the stellar lines themselves. The local continua of the spectra were fitted and normalised by a 4th-order Legendre function with the `IRAF` task `continuum`.

Irrespective of the width of the entrance slit – if one opens it to more than the width (*FWHM*) corresponding to the stellar image – the factual entrance slit becomes the star itself. So for our case, the effective spectral resolution was higher then $R = 50\,000$, but not well constrained. Thus for the sake of consistency all spectra are degraded to the worst case, that is a spectral resolution of $R = 50\,000$.

[4] The order of the stars given here and throughout the paper is based on the strengths of the CO and OH bands, which can be seen in Fig. 3.

[5] During early science verification, detectors 1 and 4 suffered some vignetting. Moreover, a quasi "odd-even"-effect, characteristic of this type of array, could not yet be mitigated by non-linear flatfielding. In the future, within the limits of the width of the Echelle order, also these detectors can be employed for precison abundance studies and to constrain the stellar continuum.

[6] IRAF is distributed by the National Optical Astronomy Observatory, which is operated by the Association of Universities for Research in Astronomy (AURA) under cooperative agreement with the National Science Foundation.

Table 1. Log of our observations. The stars are taken from Arp (1965).

Star	RA	dec	H	$t_{\rm exp}$	*SNR*
Arp 4203	18 03 23.6	–30 01 59	9.2	200 s	80
Arp 4329	18 03 28.4	–29 58 42	11.1	1800 s	95
Arp 1322	18 03 49.4	–30 01 54	10.3	600 s	110

4. Analysis

The spectral resolution is high enough for spectral lines to be resolved. Furthermore, in the near-IR wavelength region there are few enough lines that many lines are not blended. This makes the abundance analysis easier, since individual, unblended lines can be studied. In the spectra observed we have identified approximately 50 CN, 40 OH, and 40 CO lines of varied quality for an abundance analysis. We determined the carbon abundance from the CO($v = 3 - 0$) band, the nitrogen abundance from a dozen suitable CN lines, and the oxygen abundance from a dozen suitable OH lines. Furthermore, many metal lines are identified and used in the analysis.

We analyse our data by modelling the stellar atmospheres of our observed stars and calculating synthetic spectra, using extensive line lists, for that atmosphere. The temperature-dependent partition functions and continuous opacities are calculated for every depth in the atmosphere. The spectral region we observed and synthesise ranges from $\lambda_{\rm air} = 15\,315$ to $15\,710$ Å. The synthetic spectrum is thereafter convolved with a macroturbulence function in order to fit the shapes and widths of the lines, including the stellar macroturbulence and instrumental broadening (given by the spectral resolution). We then derive elemental abundances by fitting the synthetic to the observed spectra by changing the atomic abundances, which are used in the calculation of the synthetic spectra and the molecular equilibria. Finally, we reiterate the method using the derived abundances in the model atmosphere calculation in order to be self-consistent.

The best fits are found by visual inspection line by line, interpolating in three synthetic spectra with incremental differences in C, N, or O abundance of 0.05 dex. For every suitable OH and CN line the best fit is determined. For the CO band a best general fit to the feature is determined. In Fig. 5 we demonstrate how clearly a difference of 0.1 dex in the abundances of C, N, or O from the observed spectra can be determined. Note, that for our bulge stars, the CO lines are relatively independent of the O and N abundances and that the OH lines are relatively independent of the C and N abundances. In contrast, the CN lines get stronger with increasing C and get weaker with increasing O. However, with well defined C and O abundances from many lines, the CN lines are mainly dependent on the N abundance. Using Arp 4329 as an example, we find the following abundances and standard deviations: *(i)* $\log\epsilon(\mathrm{C}) = 7.42 \pm 0.05$ from the CO band; *(ii)* from the many OH we find $\log\epsilon(\mathrm{O}) = 8.25 \pm 0.03$; and *(iii)* from the many CN lines $\log\epsilon(\mathrm{N}) = 7.23 \pm 0.05$, the latter two with a standard deviation of the mean of 0.01. Hence, we find a typical standard deviation of 0.05 dex for the observational uncertainties.

Next, we will discuss the model atmospheres, the stellar parameters, the spectrum synthesis, and the line data.

4.1. Model atmospheres

We use model atmospheres provided by the MARCS code (Gustafsson et al. 2008). These hydrostatic, spherical model photospheres are computed on the assumptions of local

thermodynamic equilibrium (LTE), chemical equilibrium, homogeneous spherically-symmetric stratification, and the conservation of the total flux (radiative plus convective; the convective flux being computed using the mixing length recipe). The radiation field used in the model generation is calculated with absorption from atoms and molecules by opacity sampling at approximately 95 000 wavelength points over the wavelength range 1300 Å−20 μm. The models are calculated with 56 depth points from a Rosseland optical depth of $\log \tau_{\rm Ross} = 2.0$ out to $\log \tau_{\rm Ross} = -5.0$. Data on absorption by atomic species are collected from the VALD database (Piskunov et al. 1995) and Kurucz and other authors (for details, see Gustafsson et al. 2008). The opacity of CO, CN, CH, OH, NH, TiO, VO, ZrO, H_2O, FeH, CaH, C_2, MgH, SiH, and SiO are included and up-to-date dissociation energies and partition functions are used.

The fundamental parameters of the star are needed as input for the model photosphere calculation. Based on optical spectra and an extensive discussion, Fulbright et al. (2006, 2007) derived these parameters for, among others, our 3 programme stars. In our analysis we use these stellar parameters, see Table 3. Fulbright et al. (2006) find a good agreement for these stars between the Kurucz models they use and MARCS models. Our models are calculated in spherical geometry, assuming a mass of 0.8 $M_\odot$. Unfortunately, the range in excitation energy for the molecular transitions in our wavelength region is not great enough to admit a good determination of effective temperature from the spectra alone. In future studies, the possibilities to extend the wavelength region in order to admit such determinations should be explored.

The iron abundances of Fulbright et al. (2007) are used in the models. In the model atmosphere calculation we have used a general [α/Fe] = 0.4 (including oxygen) for the two most metal-poor stars, whereas for Arp 1322 we use [α/Fe] = 0.2 (based on the discussion by Melendez et al. 2009, in prep.). We also use specific abundances for several elements. *(i)* The C, N, O, Si, S, Ti, Cr, and Ni abundances are derived from our spectra. *(ii)* The logarithmic Mg, Al, and Na abundances are taken from the analysis by Fulbright et al. (2007) for these stars, which are {7.44, 6.34, 5.89}, respectively for Arcturus, {6.74, 5.63, 5.24} for Arp 4203, {7.06, 5.85, 5.56} for Arp 4329, and {7.52, 6.65, 6.36} for Arp 1322, on the usual scale where the hydrogen abundance is set to 12. Among these abundances Mg is important as an electron donor and may therefore affect the equivalent widths of spectral lines through the continuous opacity, which is mainly due to H^-, while Al and Na are less significant. In a model of, for instance Arp 1322, the most important electron donors at $\tau_{\rm Ross} \sim 1$ are, in order of importance, Mg, Si, Fe, Al, H, Na, and Ca. The further out in the atmosphere, the relatively more important Al and Na become. Mg and Fe are, however, still the most important contributors in shallower layers.

The atomic opacity files used in a MARCS calculation are pre-calculated in a grid. The ones used for our stars are thus files with a general metallicity of [Fe/H] = −1.25, −1.00, and −0.25, for Arp 4203, Arp 4329, and Arp 1322, respectively. The [α/Fe] enhancement in the pre-tabulated opacity files are 0.4, 0.4, and 0.2, respectively. Furthermore, the opacity files are calculated with a microturbulence parameter of 2 km s^{-1}.

4.2. Synthetic spectra

For the purpose of analyzing our observations, we have generated synthetic spectra, also calculated in spherical geometry, based on these model photospheres. Calculating a synthetic spectrum from a given line list and given abundances, is done with the program BSYN v. 7.06, and calculating an abundance for an element from measured equivalent widths, is done with the program EQWI v. 7.05. These programs are based on procedures from the MARCS code.

The same general metallicity ([Fe/H]), [α/Fe], and individual abundances of the specified elements, are used as in the calculation of the model atmosphere. In addition a $^{12}C/^{13}C = 24$ (96% ^{12}C) is used for the bulge stars, and $^{12}C/^{13}C = 9$ for α Boo. For elements which are not trace elements, but whose abundances affect the model structure, we iteratively change the abundance in the calculation of the model atmospheres, in order to be self-consistent.

We have synthesised the entire observed wavelength range. We calculate the radiative transfer for points in the spectrum separated by ∼0.5 km s^{-1} (corresponding to a resolution of R = 600 000), although the final resolution is lower. With microturbulence velocities of 1.5 km s^{-1} or more, this will ensure an adequate sampling in the generation of the synthetic spectra.

Finally, to match the observed line profiles, we introduce the customary artifice of a macroturbulent broadening, with which we convolve our synthetic spectra with a radial-tangential function (Gray 1992). This extra broadening also includes the instrumental profile and does not change the equivalent widths of the lines. We find that we need a macroturbulence of $\xi_{\rm macro}$ = 6.2, 5.8, and 6.2 km s^{-1} (*FWHM*) for Arp 4203, Arp 4329, and Arp 1322, respectively.

4.2.1. Atomic and molecular line lists

The line lists needed for the generation of the synthetic spectra consist of tables of wavelengths, excitation energies of the lower state of the transition, line strengths in the form of oscillator strengths, and the statistical weight of the upper level of the transition for molecules and atoms. Depending on the transition, the atomic line lists also provide the collisional line-broadening computed according to the collisional broadening theory by Anstee & O'Mara, (see for instance Anstee & O'Mara 1995; Barklem et al. 2000; Barklem & Aspelund-Johansson 2005) or the damping enhancement factor for van der Waals broadening. Furthermore, the lists provide the radiative damping ($\Gamma_{\rm rad}$), and the electronic orbitals and designation of the levels involved in the transition.

The atomic line list is compiled from the VALD database (Piskunov et al. 1995). In addition, we have determined "astrophysical gf-values" by fitting atomic lines in synthetic spectra to the solar spectrum (Livingston & Wallace 1991), see Fig. 1 and Table 7. The lines fitted were, among others, some Fe, Ni, S and Ti lines.

The lines which are too weak in the solar spectrum but visible in the α Boo spectrum are fitted to the "summer" version of the α Boo[7] IR atlas of Hinkle et al. (1995a), see Fig. 2 and Table 7. In principle, there are, in the wavelength range observed, 11 Si lines (1 saturated), 7 Ti (2 saturated), 4 S, 5 Ni, 1 Cr, and many Fe lines to be used for an abundance analysis in bulge giants similar to ours. A few lines are avoided, such as the Ti lines at λ15 334.8 and 15 543.8 Å ($\log W/\lambda \sim -4.9$) which are saturated and therefore less sensitive to the abundance and quite sensitive to the microturbulence. The parameters of our α Boo model are adopted as in Fulbright et al. (2007), namely, $T_{\rm eff}$ = 4290 K, $\log g$ = 1.55 (cgs), [Fe/H] = −0.50, [α/Fe] = 0.4,

[7] The fundamental parameters of Arcturus are closer to those of our programme stars.

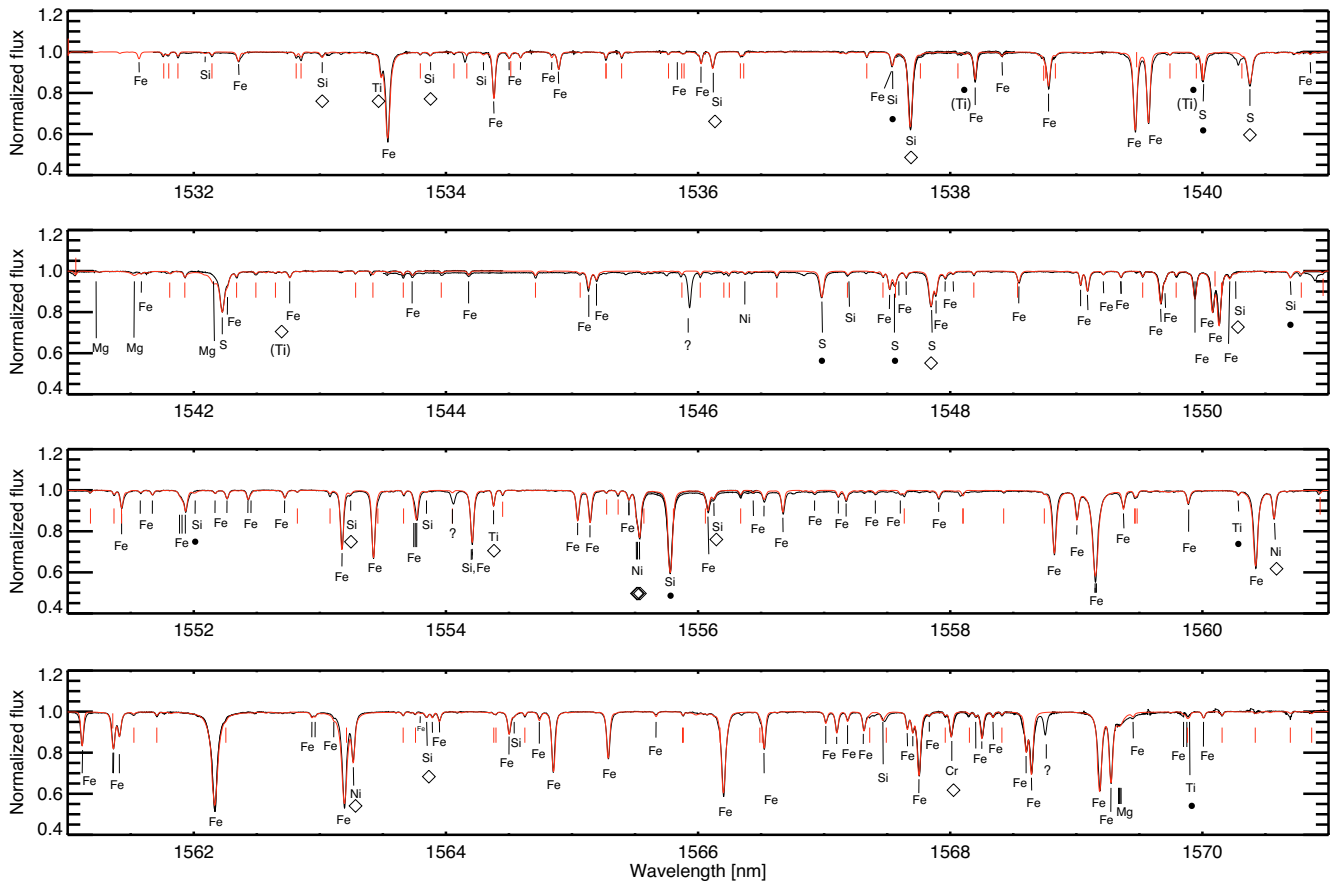

Fig. 1. Observed Sun spectrum (Livingston & Wallace 1991) in the *H* band is shown with a full, black line. Our best synthetic spectrum is shown in red. All synthetic lines which are deeper than 0.97 of the continuum are marked. Metal lines are shown below the spectrum. The metal lines are fitted to the solar atlas by changing their line strengths given the abundances compiled by Grevesse & Sauval (1998). The lines used for an abundance analysis in the stellar spectra are shown with diamonds (for good unblended lines) and dots (for blended, slightly less sensitive lines). A few of the good lines are too strong and therefore very sensitive to the microturbulence and less useful for determining the corresponding abundance. A few Ti lines which are seen in our stellar spectra are not visible in the solar spectrum. CN lines are indicated below the spectrum by red lines.

and $\xi_{\rm micro} = 1.7$. The abundances of α Boo of Mg, Al, Na, Si, Ti, and Ca are taken from Fulbright et al. (2007). The synthetic spectra are convolved with a macroturbulence parameter of 4 km s^{-1} for the comparison with the atlas. It would appear that the atlas was normalised such that the very wide Bracket hydrogen lines were removed. Therefore these were not included in the synthetic spectrum calculations, which will have some effects on the line widths.

The molecular line lists are given for all isotopic combinations that are relevant. The molecular lists included are, for CO (Goorvitch 1994), SiO (Langhoff & Bauschlicher), CH (Jørgensen et al. 1996), CN (Jørgensen & Larsson 1990; Plez 1998, private communications), OH (Goldman et al. 1998), and C_2 (Querci et al. 1971; Jørgensen 2001, private communications). The accuracy and the completeness of these line lists are discussed in Decin (2000). For the molecules, the line lists were adopted as they are and instead of modifying the gf values, the abundances of $\log \epsilon_{\rm O} = 8.76$ (from OH lines), then $\log \epsilon_{\rm C} = 8.06$ (from CO lines) and last $\log \epsilon_{\rm N} = 7.67$ (from CN lines) were obtained from the Arcturus atlas. These values are in fair agreement with the values found by Decin et al. (1997) and used in Ryde et al. (2002), namely $\log \epsilon_{\rm O} = 8.67$, $\log \epsilon_{\rm C} = 7.90$ $\log \epsilon_{\rm N} = 7.55$. The OH and CO lines are not seen in the Solar atlas and can therefore not be checked. In contrast to the case for the OH and CO lines, the wavelengths of the CN lines very often seem to be wrong, giving rise either to too strong or too weak features, and sometimes features where there are no observed lines at all. Therefore the judgement of the general fit for the CN lines will be uncertain. A few obvious shifts were made. The CN lines in the Sun seem to become too weak when our C, N, and O abundances of 8.41, 7.80, and 8.66, respectively (Asplund et al. 2005), are assumed. This improves if instead the Grevesse & Sauval (1998) abundances are used. This might perhaps be expected considering the 3D modelling origin of former abundances and the 1D plane-parallel models used here.

5. Discussion

In Fig. 3 we show our observations of the three observed bulge giants and the Arcturus spectrum, together with our final synthetic spectra. Only data from the detector array with the highest *SNR* are shown here (the third one of four). The bulge-star spectra are shown in the order of increasing metallicity and CO-band strength. The fits are, in general, very good. It is obvious that there are numerous, clean molecular-lines of CO, CN, and OH available in this region from which the C, N, and O abundances, as well as the important C-N-O molecular equilibria, can be determined. This should be compared with the scarcity of relevant lines in the optical region.

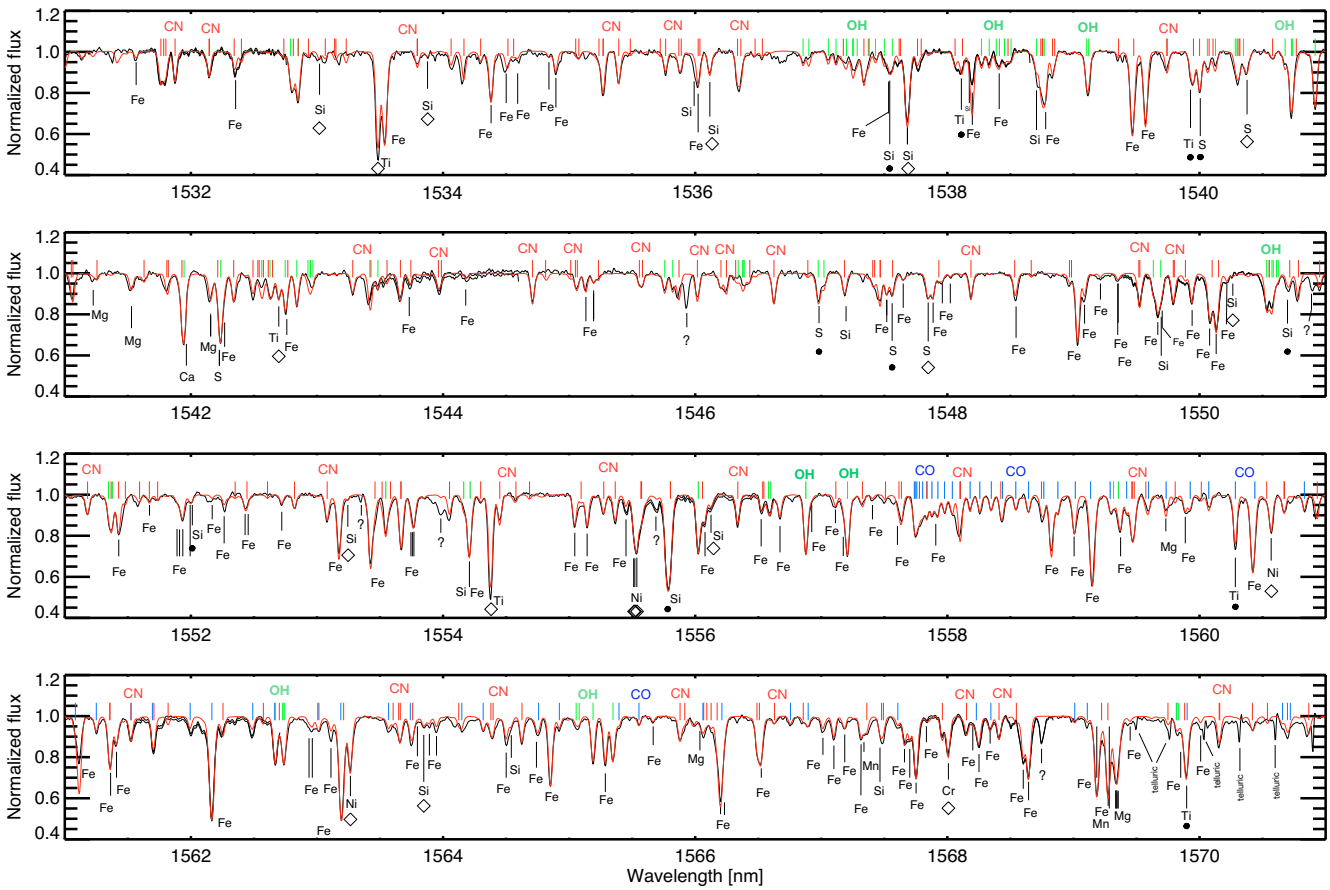

Fig. 2. Observed Arcturus spectrum (Hinkle et al. 1995b) is shown with a full, black line. Our best synthetic spectrum is shown in red. All synthetic lines which are deeper than 0.97 of the continuum are marked. Metal lines are indicated below the spectrum. A lot of them are blended with molecular lines and some are not visible as such, but these are marked anyway since they do contribute to the spectral feature. The gf values of metal lines visible in the solar spectrum are determined from Fig. 1. The other lines are fitted in the Arcturus atlas by changing their line strengths given the abundances deduced by Fulbright et al. (2007). Molecular lines are indicated above the spectrum (red for CN, blue for CO and green for OH). Some well-suited molecular lines for an abundance determination (i.e. of suitable strength and unblended) are indicated with CN, CO, and OH respectively. As can be seen the weak and strong OH lines can not be fitted with the same abundance. The stronger OH(v = 2−0, 3−1) lines indicate an abundance of $A_{\rm O}$ = 8.79 and the weaker OH(v = 4−2) ones require an oxygen abundance 0.1 dex lower to be fitted. This difference is not understood but will be investigated later.

Since the uncertainties in the abundances derived from molecular lines due to uncertainties in the fundamental parameters are of importance, we append a discussion of the sensitivities of the derived abundances to the fundamental parameters in Appendix A.

5.1. Uncertainties in the derived C, N, and O abundances

For a typical uncertainty of +100 K, for a model at 4000 K, uncertainties of $\Delta A_{\rm C}$ = +0.05 dex, $\Delta A_{\rm N}$ = +0.06 dex, and $\Delta A_{\rm O}$ = +0.14 dex are found. A typical uncertainty in $\log g$ of +0.2 dex, gives correspondingly, also at $T_{\rm eff}$ = 4000 K, $\Delta A_{\rm C}$ = +0.08 dex, $\Delta A_{\rm N}$ = −0.02 dex, and $\Delta A_{\rm O}$ = +0.03 dex. Similarly, for an uncertainty in the microturbulence of +0.5 km s^{-1}, one gets $\Delta A_{\rm C}$ = −0.02 dex, $\Delta A_{\rm N}$ = −0.07 dex, and $\Delta A_{\rm O}$ = −0.03 dex. Low values are, indeed, expected for weak lines, such as these typical lines used in this test. Finally, uncertainties in the metallicity and [α/Fe] of +0.1 dex yield uncertainties in the C, N, and O abundances of +0.08 dex and +0.02 dex, respectively. Thus, we estimate the total internal uncertainties in the derived C, N, and O abundances, assuming uncertainties in the stellar parameters to be uncorrelated, to be approximately $\Delta A_{\rm C} = \sqrt{0.05^2 + 0.08^2 + 0.02^2 + 0.08^2 + 0.02^2} = 0.13$, $\Delta A_{\rm N} = \sqrt{0.06^2 + 0.02^2 + 0.07^2 + 0.08^2 + 0.02^2} = 0.13$, and $\Delta A_{\rm O} = \sqrt{0.14^2 + 0.03^2 + 0.03^2 + 0.08^2 + 0.02^2} = 0.17$. As a comparison, the standard deviations in the determinations of the C, N, and O abundances from the many observed CO, CN, and OH lines for a given model are small, less than 0.05 dex.

A source of uncertainty for N abundances might also be the dissociation of energy of CN, which is here, following Costes et al. (1990) set to D_0 = 7.77 eV. This quantity used to be highly uncertain. We note, however, that Pradhan et al. (1994) found the value D_0 = 7.72 ± 0.04 from multireference configuration-interaction calculations, which also agrees with experimental results of Huang et al. (1992) of 7.74 ± 0.02. Thus, at least differentially to Arcturus, the errors in N abundances due to this should be negligible.

Whereas both weak and strong OH lines are fitted nicely in Arp 4329 and Arp 1322, the strong ones are too weak in the model of Arp 4203 and the weak ones too strong. The same is found for the Arcturus spectrum. This problem can not be solved by the modification of effective temperatures, and is thus not understood but will be investigated later.

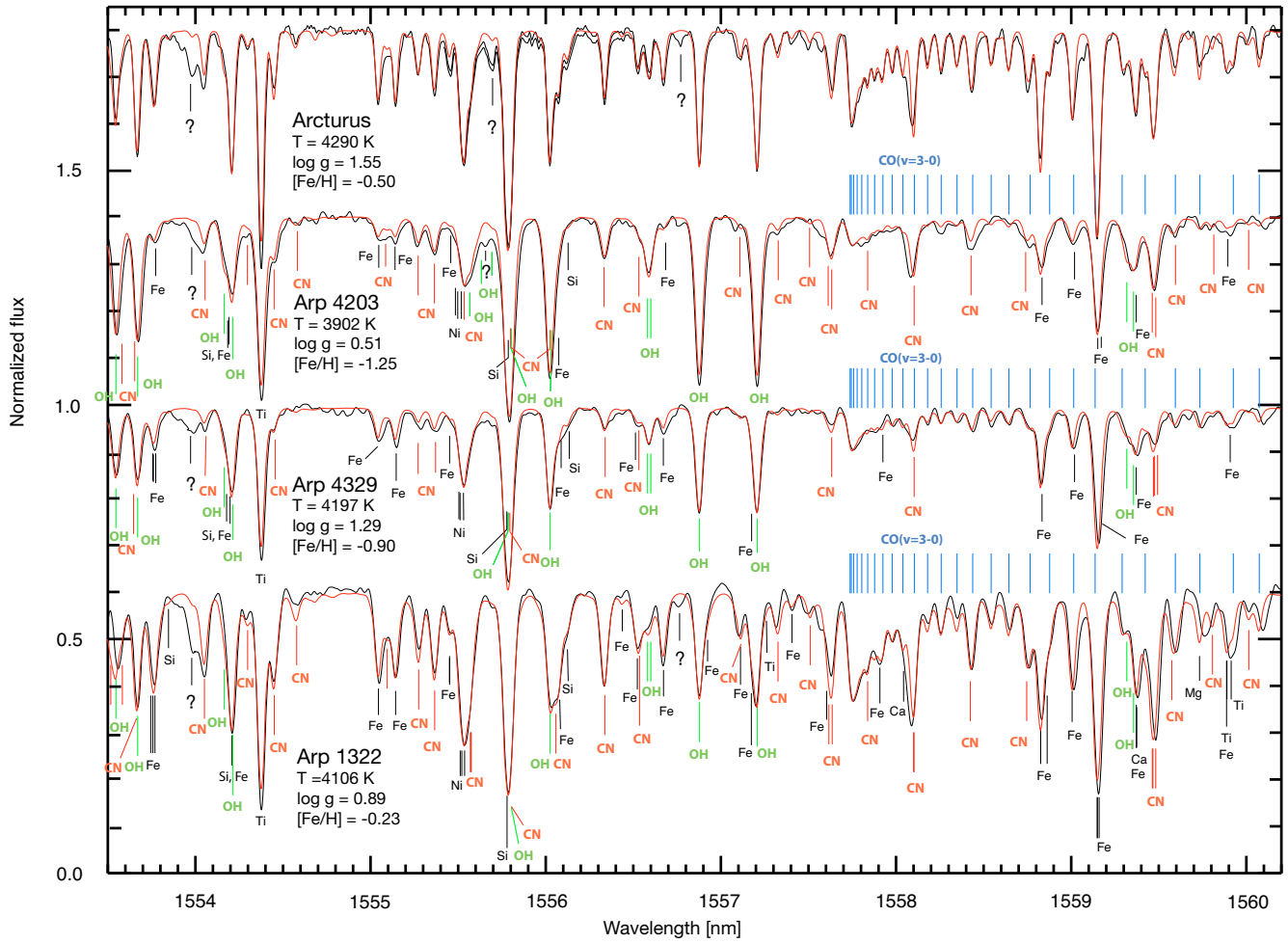

Fig. 3. Sections of the observed CRIRES spectra of the three bulge giants Arp 4329, Arp 4203, and Arp 1322 in Baade's Window are shown with full, black lines. For comparison, the Arcturus atlas spectrum (Hinkle et al. 1995b) is also shown. The parts of the spectra which have the highest signal-to-noise ratios are shown. In these parts the C, N, and O elements can be determined. Our best synthetic spectra is shown in red. All synthetic lines which are deeper than 0.97 of the continuum are marked. A few features are not identified in the Arcturus spectrum and are labelled with question marks. These features also show up in the bulge-star spectra.

5.2. Abundances

A part of the analysis is presented in Ryde et al. (2007), where we provide our preliminarily derived elemental abundances. Our new resulting abundances of C, N, O, Ti, Si, S, Cr, Ni, and Fe are presented in Tables 2 and 4. As a comparison the abundances for the same stars determined by Fulbright et al. (2007, 2006) are also provided in the tables. Typical uncertainties for the abundances derived from atomic lines are of the order of 0.1 dex and of the order of 0.15 dex from molecular lines. The uncertainties in the derived oxygen abundances by Fulbright et al. (2007) are approximately 0.15 dex (from the [OI] λ6300 line) and 0.1 dex for Si and Ti. A good agreement is found between our near-IR abundances of O, Ti, Si, and Fe and the abundances from Fulbright et al., an analysis based on optical spectra. The largest discrepancy, albeit within the uncertainties, is in the oxygen abundance, which is not surprising. The good agreement is reassuring for future analysis of stars for which only near-IR spectra will exist, for instance, analyses of bulge stars closer to the Galactic plane. It should be noted, however, that a general problem in determining elemental abundances for stars with only near-IR spectra is the temperature sensitivity of the molecular lines and the difficulties in the determination of the stellar parameters.

In Table 4 the relative abundances of the elements for Arcturus and the three bulge giants relative to the solar values are given. We see that Arcturus has quite a large over-abundance of [O/Fe] which is approximately three times that expected for disk stars at [Fe/H] = −0.5. The [O/Fe] for the three bulge stars fits very well with the trend discussed in Meléndez et al. (2008). Our two "metal-poor" stars lie on the plateau defined by both disk and halo stars. Our determination of the [O/Fe] in Arcturus lies at the high end, mostly populated by thick disk stars (see Fig. 2 in Meléndez et al. 2008). Our low [O/Fe] value for Arp 1322 with [Fe/H] = −0.25 corroborates the finding of Meléndez et al. (2008) that there is no obvious difference between the oxygen abundance in bulge stars and those in thick disk stars. More stars are, however, needed in order to confirm this trend. Note that in a recent paper Chiappini et al. (2008) compare, among others, the oxygen abundances derived from planetary nebulae (PNe) and giants in the bulge and find an interesting discrepancy that the abundances determined from giant star spectra are systematically higher by 0.3 dex. They conclude that this discrepancy may be caused by systematic uncertainties in either the PNe or giant star abundance determinations, or both.

The carbon abundances are all depleted in our bulge giants, and nitrogen is enhanced. In Arp 4329 and Arp 1322 the C+N seems, however, conserved. This is, indeed, expected for

Table 2. Abundances for Arcturus and the three bulge giants.

Star	Ref.	log ε(C)[a] [dex]	log ε(N) [dex]	log ε(O) [dex]	log ε(Ti) [dex]	log ε(Si) [dex]	log ε(S) [dex]	log ε(Cr) [dex]	log ε(Ni) [dex]	log ε(Fe) [dex]
Arcturus	this work	8.06	7.67	8.76	4.68	7.35	6.94	5.17	5.78	7.00
	Fulbright et al.	–	–	8.67	4.68	7.39	–	–	–	6.95
	difference	–	–	0.09	0.00	−0.04	–	–	–	0.05
Arp 4203	this work	6.62	7.70	7.71	3.98	6.75	6.26	4.28	5.12	6.25
	Fulbright et al.	–	–	7.55	4.03	6.82	–	–	–	6.20
	difference	–	–	0.16	–0.05	−0.07	–	–	–	0.05
Arp 4329	this work	7.42	7.23	8.25	4.33	7.15	6.81	4.77	5.41	6.60
	Fulbright et al.	–	–	8.16	4.30	7.14	–	–	–	6.55
	difference	–	–	0.09	0.02	0.01	–	–	–	0.05
Arp 1322	this work	7.93	8.10	8.61	4.87	7.52	7.35	5.62	6.02	7.33
	Fulbright et al.	–	–	8.80	4.84	7.43	–	–	–	7.22
	difference	–	–	−0.19	0.03	0.09	–	–	–	0.11

[a] log ε(X) = log n_X/n_H + 12, where log n_X is the number density of element X.

Table 3. Stellar parameters from Fulbright et al. (2006, 2007).

Star	T_{eff} [K]	log g cgs	[Fe/H]	ξ_{micro} [km s^{-1}]	[α/Fe]
Arp 4203	3902	0.51	−1.25	1.9	0.4
Arp 4329	4197	1.29	−0.90	1.5	0.4
Arp 1322	4106	0.89	−0.23	1.6	0.2

giants that have ascended the giant branch for the first time. They have experienced CN-cycling in their interiors (with ^{14}N and ^{13}C as products) and experienced the first dredge-up. The giant Arp 4203 shows a large depletion of carbon and a large enhancement of nitrogen. Further, the [C+N/Fe] is non-solar, making this giant special. Fulbright et al. (2007) also note the peculiarity of this giant. They argue that it is a cluster member of NGC 6522 based on their oxygen, high sodium, and aluminum abundance pattern. A possibility is that this giant has experienced nuclear processing in H-burning shells, with subsequent dredge-up of material to the surface. This burning would also be responsible for the O-Na correlations in globular clusters. The high [C+N/Fe] we find may fit with this picture, since one expects an increased [N/Fe] ratio due to CNO-cycling (Gratton et al. 2004; Meléndez et al. 2008). We also find that Arp 4203 has an excess of O relative to Fe ([O/Fe] = 0.3), which may, however, be slightly lower than the assumed general α-element enhancement of +0.4. The sum of the abundances of C, N, and O ([C+N+O/Fe] ∼ 0.4) is close to that expected from a non-processed old star, formed with an excess of oxygen and α elements relative to iron. Thus, if the carbon and nitrogen abundances are correct, this implies that the oxygen abundance in this star should actually not be used to represent the unprocessed value for this bulge giant.

As regards the α elements Si and Ti we find abundance values which agree with those of Fulbright et al. (2007). Our sulphur abundances are the first determinations for bulge stars as far as we know. All [S/Fe] ratios are relatively high, also for our most metal-rich star ([S/Fe] = +0.4 at [Fe/H] = −0.2). This implies a high star-formation rate in an early phase of the bulge evolution as discussed in the Introduction.

The Cr abundance is based on one line which introduces uncertainties due to the continuum fitting and a CN line blending into the line. This is true in particular for the most metal-rich star of our sample. Thus, given the uncertainties, we cannot say whether the Cr abundance follows the general metallicity or not. This is also true for our abundance result for Ni.

It is interesting to note that lines from Si, S, Ni, and Cr in α Boo are nearly of the same strength as in the Sun. The Sun is more metal-rich and hotter which would increase the strength of these highly excited lines (χ_{exc} = 5−8 eV). However, the continuous opacity due to H$^-$ is also larger, which thus compensates for this effect. Some Fe lines are stronger, others slightly weaker, and the Ti lines are much stronger in Arcturus.

6. Conclusions and outlook

Stellar surface abundances in bulge stars can be extensively studied in the near-IR, due to lower extinction. In particular, the abundances of the C, N, and O elements are advantageously studied in the near-IR compared to the optical wavelength region, due to numerous CO, CN, and OH lines. All these molecules are observable in the same part of the spectrum and can therefore be studied simultaneously in order to determine the molecular equilibria properly. Here, we present the first three CRIRES spectra of bulge stars, observed during the *science verification observations* of the CRIRES spectrometer at the *VLT*. We show that we can determine the C, N, and O abundances from molecular lines, with uncertainties of ∼0.15 dex, which are mainly due to uncertainties in the stellar parameters. Unfortunately, the range in excitation energy for the molecular lines is not great enough for determinations of effective temperatures from our spectra. The possibilities to extend the wavelength region in order to admit such determinations should be explored.

For oxygen, titanium, iron, and silicon, we show a good agreement between near-IR and optically determined abundances in stars in Baade's window, stars which can be observed in both wavelength ranges. For the two of our stars that show an unprocessed oxygen abundance, the [O/Fe] trend corroborates the idea that there is no significant difference between the oxygen abundances in bulge and thick disk stars. The abundance of the α element sulphur indicates a high star-formation rate in an early phase of the bulge evolution.

It will be very important to extend the analysis to more stars and especially to stars in other regions of the Galactic bulge, such as in the Galactic plane, in order to get a proper handle on the formation and evolution of the bulge. In these regions the optical extinction is high which permits observations only in the near-IR. Near-IR, high-spectral-resolution spectroscopy offers a promising methodology to study the whole bulge to give clues to its formation and evolution.

The observations presented here have demonstrated the feasibility and power of precision abundance measurements in the

Table 4. Abundances for Arcturus and the three bulge giants relative to the Sun, where $[X/Fe] = \{\log\varepsilon(X) - \log\varepsilon(Fe)\}_{star} - \{\log\varepsilon(X) - \log\varepsilon(Fe)\}_{\odot}$.

Star	Ref. Star	[C/Fe]	[N/Fe]	[C+N/Fe]	[O/Fe]	[Ti/Fe]	[Si/Fe]	[S/Fe]	[Cr/Fe]	[Ni/Fe]	[Fe/H]
Arcturus	this work[a]	0.15	0.37	0.20	0.60	0.16	0.30	0.24	0.00	0.03	–0.50
	Fulbright et al.[b]	–	–	–	0.51	0.16	0.34	–	–	–	–0.50
Arp 4203	this work[a]	−0.54	1.15	0.48	0.30	0.21	0.45	0.31	−0.14	0.12	−1.25
	Fulbright et al.[b]	–	–	–	0.14	0.26	0.52	–	–	–	−1.25
Arp 4329	this work[a]	−0.09	0.33	0.03	0.49	0.21	0.50	0.51	0.00	0.06	−0.90
	Fulbright et al.[b]	–	–	–	0.40	0.18	0.49	–	–	–	−0.90
Arp 1322	this work[a]	−0.25	0.53	0.05	0.18	0.08	0.20	0.38	0.18	0.00	−0.17[c]
	Fulbright et al.[b]	–	–	–	0.37	0.05	0.11	–	–	–	−0.23

[a] We have used the following solar abundances: $\log\varepsilon(C) = 8.41$, $\log\varepsilon(N) = 7.80$, $\log\varepsilon(O) = 8.66$, $\log\varepsilon(Fe) = 7.50$, $\log\varepsilon(Ti) = 5.02$, $\log\varepsilon(Si) = 7.55$, $\log\varepsilon(S) = 7.20$, $\log\varepsilon(Cr) = 5.67$, and $\log\varepsilon(Ni) = 6.25$.
[b] Fulbright et al. used the following solar abundances: $\log\varepsilon(O) = 8.69$, $\log\varepsilon(Fe) = 7.45$, $\log\varepsilon(Ti) = 4.92$, and $\log\varepsilon(Si) = 7.54$. For the sake of comparison we have scaled their values to the solar values we have used.
[c] The [Fe/H] from this work is determined from FeI lines in the CRIRES wavelength region, but not used as the metallicity in the models.

H-band. Some technical shortcomings of these early science verification observations have triggered the investigation into better non-linear flat fielding. Moreover this work has triggered the search for ways to improve throughput and efficiency. It has therefore been important for defining the scientific requirements and the scope of the CRIRES upgrade plan, and in this context changing the Echelle format by procuring a custom-ruled grating. Then it will be possible to use all pixels in the spectrograph focal plane without compromises.

Acknowledgements. The anonymous referee is thanked for valuable comments. We would also like to thank the CRIRES science verification team for their work on CRIRES and for the execution of the observations. N.R. is a Royal Swedish Academy of Sciences research fellow supported by a grant from the Knut and Alice Wallenberg Foundation. Funds from Kungl. Fysiografiska Sällskapet i Lund are acknowledged. B.E., B.G., and K.E. acknowledge support from the Swedish research council, VR. Karin Ryde is thanked for reading through the manuscript and correcting the English.

Appendix A: Sensitivities in the derived abundances to the stellar parameters

In order to test how the derived abundances from a molecular line with a given equivalent width changes for uncertainties in the fundamental parameters of a star, a program EQWIMO v.1.0 was written, based on the MARCS code. The code needs molecular line lists and information on which atom in a molecule the abundance is to be solved for. Thus, an estimate of the sensitivities of the derived carbon, nitrogen, and oxygen abundances from the CO, CN, and OH lines to the fundamental stellar parameters can be obtained by analyzing typical molecular lines of specific strengths and deriving the abundances they would yield for different stellar parameters. For this exercise we have assumed that the stellar parameters are uncorrelated. The C, N, and O abundances are determined simultaneously for a change in the parameters, by iteratively determining one at a time. The program recalculates the molecular equilibria for every iteration. Only a few iterations are needed to reach convergence. Apart from being affected by the temperature change, the abundances derived from the molecular lines are also affected by the changes in the C, N, and O abundances through the molecular equilibria. This is especially the case for the derived nitrogen abundance. In the models that we have generated for this exercise, we have used $\log\epsilon_C = 8.32$, $\log\epsilon_N = 8.00$, and $\log\epsilon_O = 8.81$. For many of the models, the derived C, N, and O abundances will be different, but this difference should not be significant for our abundance results. We have analysed typical CO, CN, and CO lines of the following strengths (equivalent widths): $W_{CO} = 60$ mÅ, $W_{CN} = 120$ mÅ, and $W_{OH} = 152$ mÅ, see Table 5.

Table 5. Test lines.

Molecule	*Wavelength* [Å]	χ_{exc} [eV]	$\log gf$ (cgs)	*W* mÅ	$\log W/\lambda$
CO	15 580.4	0.37	−7.44	60	−5.4
CN	15 563.4	1.15	−1.14	120	−5.2
OH	15 568.8	0.30	−5.29	152	−5.0

In Fig. 4, the abundances of the C, N, and O elements derived from these typical lines at 1.5 μm are shown for different effective temperatures, surface gravities, and metallicities, but for given line strengths. We can see that the oxygen abundance is most temperature sensitive. Both the CO and OH lines are of low excitation and therefore not much affected by the temperature for their excitation. The temperature behaviour of the abundances derived from these lines is mainly caused by the increasing dissociation of the molecules (more for OH, which has the lowest dissociation energy of the three molecules) as the temperature rises. Fewer molecules are available at higher temperatures, which means that the abundances of the constituting atoms have to be higher for a given equivalent width of the molecular line. The CN line, which has an excitation energy of its lower level of 1.15 eV, is more sensitive to the temperature for its excitation. As the temperature increases more CN is excited to the lower level of the CN line, which means that a lower abundance is needed for a given equivalent width. The behaviour of the derived nitrogen abundance from CN is governed by this effect, and by the increased dissociation of the molecule as the temperature increases, but also by the increase of the carbon abundance (which increases the CN abundance) and the large increase of the oxygen abundance (which increases the NO abundance and decreases the CN abundance). In sum, more nitrogen is needed for a given CN line strength as the temperature rises. In all these cases the continuous opacity does not change very much. Since the line strengths are proportional to the ratio of the line to continuous opacities, also the continuous opacity has to be discussed when analysing the changes in line strength due to abundance changes. At 1.5 μm it is almost solely due to H^- bound-free and free-free processes (more than 98%).

From Fig. 4, we can also note that the carbon abundance derived from the CO line increases with increasing surface gravity, whereas the oxygen abundance derived from the OH line is nearly independent of a change in $\log g$. The reason is that for an increase of the surface gravity from say $\log g = 1.0$ to

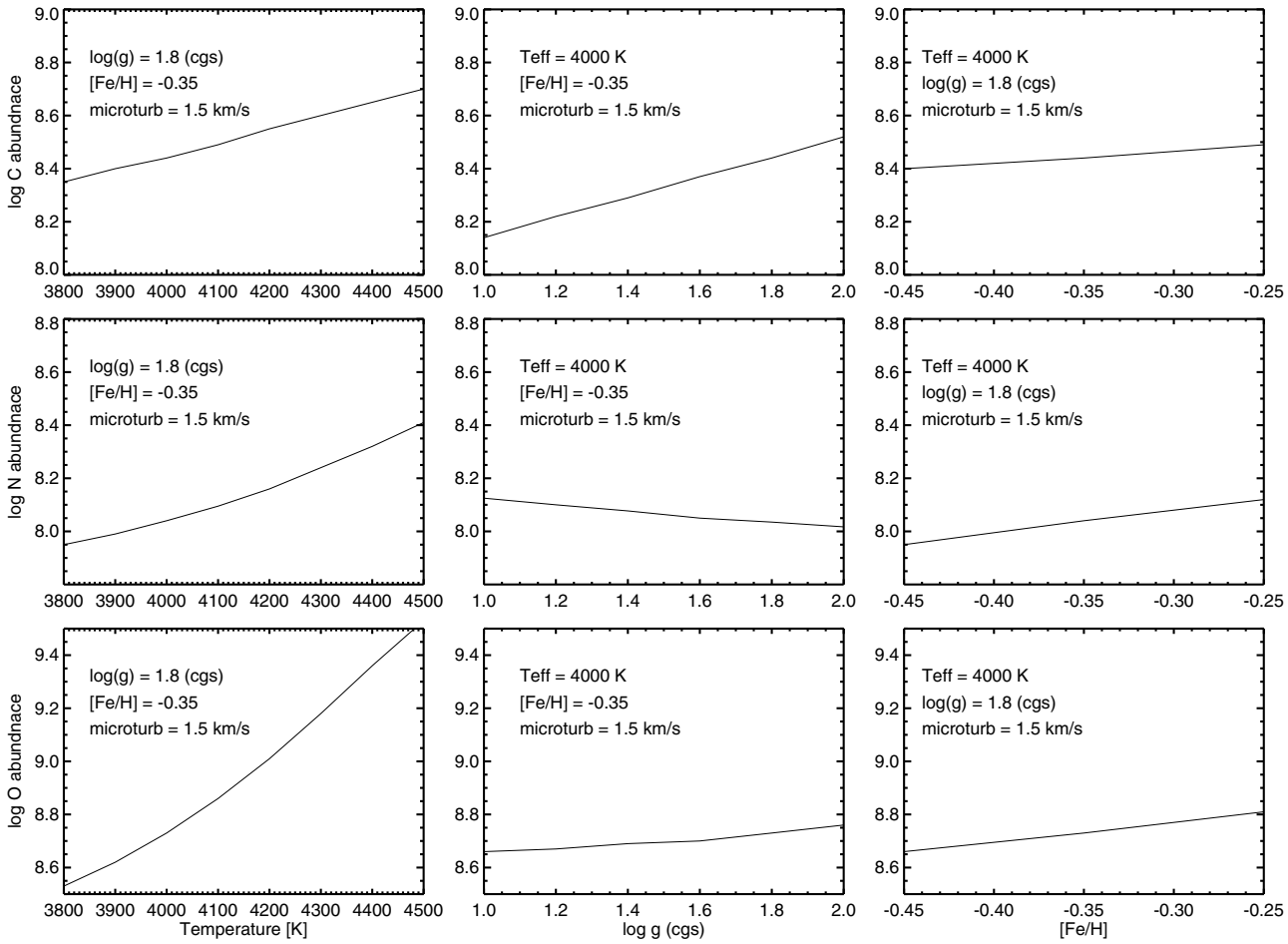

Fig. 4. The derived abundances of oxygen, carbon, and nitrogen for different temperatures, surface gravities, and metallicities for given typical CO, CN, and OH lines at 1.5 μm of the following strengths (equivalent widths): $W_{\rm CO}$ = 60 mÅ, $W_{\rm CN}$ = 120 mÅ, and $W_{\rm OH}$ = 152 mÅ. To facilitate comparisons, the different panels are in relative ordinate scale, spanning an order of magnitude in abundance.

$\log g = 2.0$, the continuous opacity increases by a factor of 3 (or 0.5 dex). However, also the partial pressure of OH ($\log P_{\rm OH}/P_{\rm g}$) at the formation depth increases by approximately the same amount, which leaves the line strengths nearly unaffected, and thus the oxygen abundances derived from a given equivalent width of the OH line will not vary greatly. However, the partial pressure of CO increases by only approximately 60% (0.2 dex). This means that the increase of the continuous opacity affects the lines more in the sense that they get weaker as the surface gravity of the stellar model increases. Hence, a larger abundance of the constituent atoms is needed for a given equivalent width. The increased carbon abundance increases the CN abundance as the gravity increases, leading to slightly lower nitrogen abundances. Finally, the C, N, and O abundances increase as the metallicity increases, since the continuous opacity increases which weakens the lines.

In Fig. 5 we show the spectral changes when changing the C, N, and O abundances by ±0.1 dex. We have chosen to take our model of Arp 4329 as a test model. The stellar parameters are given in Table 3, and, more importantly, the original C, N, and O abundances are those given in Table 2. Difference in abundances of this magnitude can clearly be detected in the observed spectra.

Of the three molecules for which we detect lines, CO is the most abundant, CO being the most stable molecule with the highest dissociation energy (see Table 6) and most carbon being locked up in CO. Next in abundance comes OH, which is easily dissociated due to a low dissociation energy. Of the nitrogen-bearing molecules, CN is the third most abundant, which makes it a trace molecule. Thus, its abundance-change is to a high degree determined by how the other three molecules, namely N_2, NH, and NO, are affected.

The continuous opacity does not change when the C, N, and O abundances are changed by 0.1 dex. Thus, with the partial pressures of the molecules in mind and noting that oxygen is more abundant than carbon and nitrogen, we can understand qualitatively the changes in Fig. 5;

- Changing the oxygen abundance affects both the OH and CN lines. Increasing the oxygen abundance increases the OH lines and decreases the CN lines by a relatively large amount. The CO lines are actually also increased, but by a very small amount. The reason for the changes is that, in the line-forming regions, the partial pressures increase by a large amount for OH and a small amount for CO, which is to be expected. Also the partial pressure of NO increases, which leads to a smaller amount of available nitrogen. Since also some extra carbon is used in increasing the number of CO molecules, there are smaller amounts of C and N left for the formation of CN, whose line strengths therefore decrease.
- When changing the nitrogen abundance, only the CN lines are affected discernibly. The partial pressures of N_2, NH, and

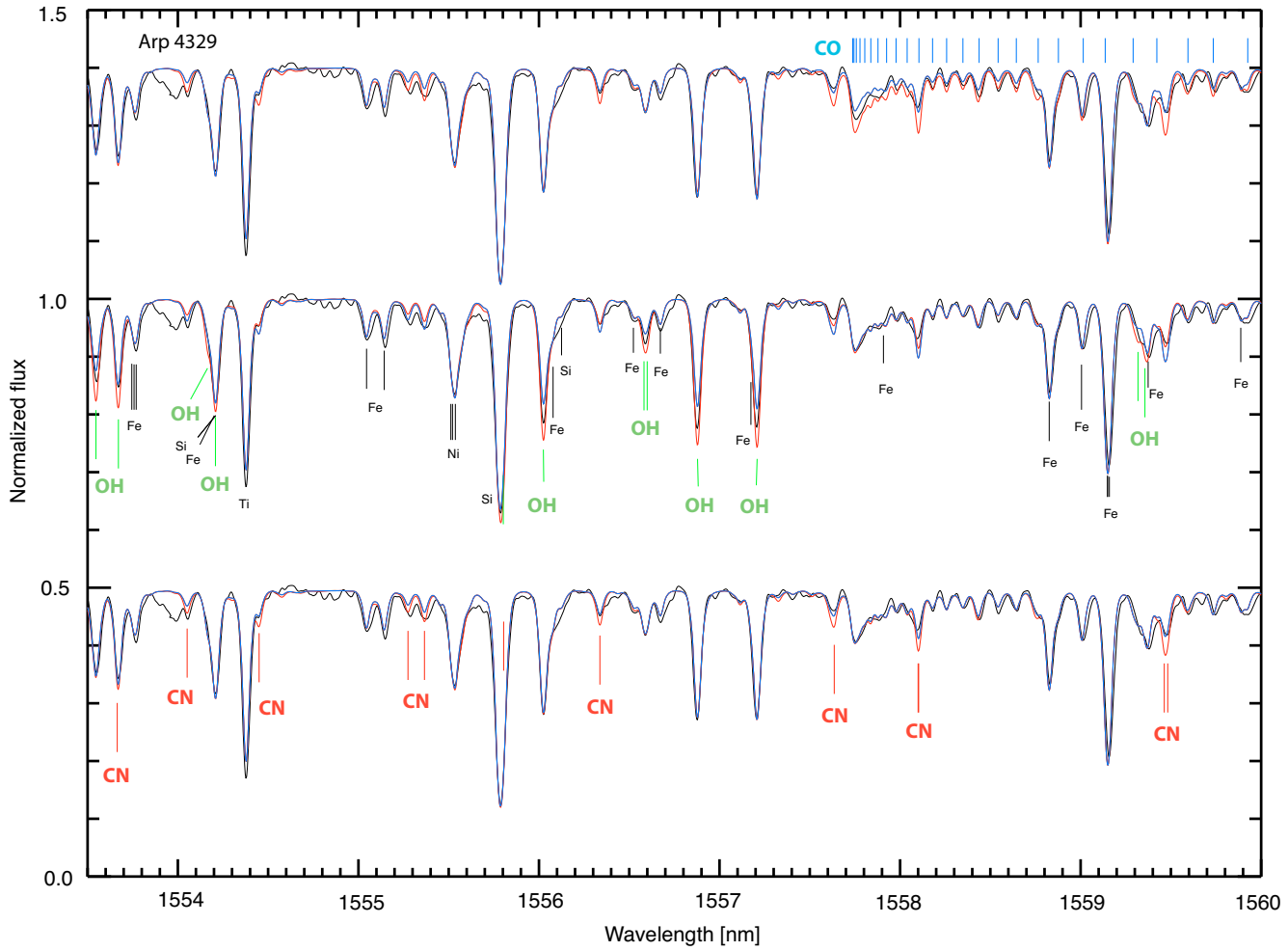

Fig. 5. Part of the observed CRIRES spectrum of the bulge giant Arp 4329 is shown with a full, black line. Synthetic spectra are shown in red and blue, with the carbon, oxygen, and nitrogen abundances, respectively, changed by +0.1 dex (red line) and −0.1 dex (blue line) relative to the best-fit abundances.

Table 6. Relative logarithmic partial pressures at $\log \tau_{\rm Ross} = 0$, and dissociation energies of some relevant molecules for a model of Arp 4329.

Molecule	$\log\{P_{\rm CO}/P_{\rm H}\}$ at $\log \tau_{\rm Ross} = 0$	D_0^0
CO	−5.8	11.09
OH	−7.0	4.39
N_2	−8.1	9.76
NH	−8.7	3.42
CN	−9.7	7.76
NO	−9.9	6.50

NO are also increased, but the OH and CO lines are not affected noticeably.

– As expected, when increasing the carbon abundance both the CO and CN lines get stronger. However, the OH pressure is not affected very much. In general, determining the oxygen abundance from OH lines can only be done if the C abundance is also know, since much oxygen is locked up in CO, and a change in the carbon abundance will affect the amount of available oxygen for OH, see point 5 in Sect. 2.1. Indeed, at solar-type C/O ratios, there is only 80% more oxygen than carbon. Changing the carbon abundance will then affect the amount of available oxygen through the formation of more CO. However, in our test model we have $\log \epsilon_{\rm O} = 8.25$ and $\log \epsilon_{\rm C} = 7.42$ (see Table 2), which means that oxygen is enhanced and carbon is reduced compared to the metallicity-scaled solar values. Thus, in our test model, which is supposed to be a model of a typical bulge giant, there is nearly seven times more oxygen than carbon, by number. Therefore, a change in the carbon abundance in a typical bulge star, with an enhanced oxygen abundance, will not change the strength of the OH lines as much as expected for a star with a solar-type carbon-to-oxygen ratio.

– To summarise and to put it in another way, for our test model, the OH lines are mainly affected by the oxygen abundance, the CO lines by the C abundance, but the CN lines are affected by the nitrogen, as well as the C and O abundances.

References

Anstee, S. D., & O'Mara, B. J. 1995, MNRAS, 276, 859
Arp, H. 1965, ApJ, 141, 43
Asplund, M., Grevesse, N., & Sauval, A. J. 2005, in Cosmic Abundances as Records of Stellar Evolution and Nucleosynthesis, ed. T. G. Barnes, III, & F. N. Bash, ASP Conf. Ser., 336, 25
Barbuy, B. 2002, in Rev. Mex. Astron. Astrofis. Conf. Ser., 14, ed. J. J. Claria, D. Garcia Lambas, & H. Levato, 29
Barklem, P. S., & Aspelund-Johansson, J. 2005, A&A, 435, 373

Barklem, P. S., Piskunov, N., & O'Mara, B. J. 2000, A&AS, 142, 467
Cardelli, J. A., Clayton, G. C., & Mathis, J. S. 1989, ApJ, 345, 245
Chiappini, C., Gorny, S., Stasinska, G., & Barbuy, B. 2008, arXiv e-prints
Costes, M., Naulin, C., & Dorthe, G. 1990, A&A, 232, 270
Cunha, K., & Smith, V. V. 2006, ApJ, 651, 491
Cunha, K., Sellgren, K., Smith, V. V., et al. 2007, ApJ, 669, 1011
Decin, L. 2000, Ph.D. Thesis, University of Leuven
Decin, L., Cohen, M., Eriksson, K., et al. 1997, in First ISO Workshop on Analytical Spectroscopy, ed. A. Heras et al., ESA SP-419, 185
Figer, D. F., Rich, R. M., Kim, S. S., Morris, M., & Serabyn, E. 2004, ApJ, 601, 319
Fulbright, J. P., McWilliam, A., & Rich, R. M. 2006, ApJ, 636, 821
Fulbright, J. P., McWilliam, A., & Rich, R. M. 2007, ApJ, 661, 1152
Goldman, A., Schoenfeld, W., Goorvitch, D., et al. 1998, JQSRT, 59, 453
Goorvitch, D. 1994, ApJS, 95, 535
Gratton, R., Sneden, C., & Carretta, E. 2004, ARA&A, 42, 385
Gray, D. F. 1992, The observation and analysis of stellar photospheres (Cambridge; New York: Cambridge University Press), 2nd Ed.
Grevesse, N., & Sauval, A. J. 1998, Space Sci. Rev., 85, 161
Gustafsson, B., Edvardsson, B., Eriksson, K., et al. 2008, A&A, 486, 951
Hinkle, K. H., & Lambert, D. L. 1975, MNRAS, 170, 447
Hinkle, K., Wallace, L., & Livingston, W. 1995a, PASP, 107, 1042
Hinkle, K., Wallace, L., & Livingston, W. C. 1995b, Infrared atlas of the Arcturus spectrum, 0.9−5.3 microns (San Francisco, Calif.: ASP)
Hinkle, K. H., Cuberly, R. W., Gaughan, N. A., et al. 1998, SPIE, 3354, 810
Hinkle, K. H., Blum, R. D., Joyce, R. R., et al. 2003, in Discoveries and Research Prospects from 6- to 10-Meter-Class Telescopes II, ed. P. Guhathakurta, Proc. SPIE, 4834, 353
Huang, Y., Barts, S. A., & Halpern, J. 1992, J. Phys. Chem., 96, 425
Jørgensen, U. G., & Larsson, M. 1990, A&A, 238, 424
Jørgensen, U. G., Larsson, M., Iwamae, A., & Yu, B. 1996, A&A, 315, 204
Käufl, H. U., Amico, P., Ballester, P., et al. 2006, The Messenger, 126, 32
Kormendy, J., & Kennicutt, Jr., R. C. 2004, ARA&A, 42, 603
Langhoff, S. R., & Bauschlicher, C. W. 1993, Chem. Phys. Lett., 211, 305
Lecureur, A., Hill, V., Zoccali, M., et al. 2007, A&A, 465, 799
Livingston, W., & Wallace, L. 1991, An atlas of the solar spectrum in the infrared from 1850 to 9000 cm-1 (1.1 to 5.4 micrometer), NSO Technical Report, Tucson, National Solar Observatory, National Optical Astronomy Observatory
McWilliam, A., & Rich, R. M. 2004, in Origin and Evolution of the Elements, ed. A. McWilliam, & M. Rauch
Meléndez, J., Barbuy, B., Bica, E., et al. 2003, A&A, 411, 417
Meléndez, J., Asplund, M., Alves-Brito, A., et al. 2008, A&A, 484, L21
Minniti, D., & Zoccali, M. 2008, in IAU Symp., 245, 323
Moorwood, A. 2005, in High Resolution Infrared Spectroscopy in Astronomy, ed. H. U. Käufl, R. Siebenmorgen, & A. F. M. Moorwood, 15
Origlia, L., & Rich, R. M. 2003, Mem. Soc. Astron. Ital., 74, 177
Origlia, L., & Rich, R. M. 2004, AJ, 127, 3422
Origlia, L., Rich, R. M., & Castro, S. 2002, AJ, 123, 1559
Ortolani, S., Renzini, A., Gilmozzi, R., et al. 1995, Nature, 377, 701
Piskunov, N. E., Kupka, F., Ryabchikova, T. A., Weiss, W. W., & Jeffery, C. S. 1995, A&AS, 112, 525
Pradhan, A., Partridge, H., & Bauschlicher Jr., C. 1994, J. Chem. Phys., 101, 3857
Querci, F., Querci, M., & Kunde, V. 1971, A&A, 15, 256
Renzini, A. 2006, ARA&A, 44, 141
Rich, R. M., & Origlia, L. 2005, ApJ, 634, 1293
Rich, R. M., Origlia, L., & Valenti, E. 2007, ApJ, 665, L119
Ryde, N., Lambert, D. L., Richter, M. J., & Lacy, J. H. 2002, ApJ, 580, 447
Ryde, N., Gustafsson, B., Eriksson, K., & Wahlin, R. 2005, in High Resolution Infrared Spectroscopy in Astronomy, ed. H. U. Käufl, R. Siebenmorgen, & A. F. M. Moorwood, 365
Ryde, N., Edvardsson, B., Gustafsson, B., & Käufl, H.-U. 2007, ed. A. Vazdekis, & R. F. Peletier, IAU Symp., 241, 260
Tody, D. 1993, in Astronomical Data Analysis Software and Systems II, ed. R. J. Hanisch, R. J. V. Brissenden, & J. Barnes, ASP Conf. Ser., 52, 173
Unsöld, A. 1955, Physik der Sternatmospharen, MIT besonderer Berucksichtigung der Sonne (Berlin: Springer), 2
Wyse, R. F. G., Gilmore, G., & Franx, M. 1997, ARA&A, 35, 637
Zoccali, M., Renzini, A., Ortolani, S., et al. 2003, A&A, 399, 931

Table 7. Line list of our 816 metal lines in the wavelength range observed. The seven columns give (1) the wavelength in air; (2) the excitation energy of the lower level; (3) $\log gf$; (4) the radiation damping parameter (when no value was available the very low value of 1.00×10^5 was used); (5) the van der Waals damping marked with an "A" when calculated according to Anstee & O'Mara (1995), Barklem et al. (2000) and references therein, Barklem & Aspelund-Johansson (2005), or Barklem P., private communication (if a number is instead given this is an empirical correction factor to the van der Waals damping computed according to Unsöld (1955)); (6) the atomic or ionic species; and (7) a star "*" when the $\log gf$ value has been modified by spectrum fits to the spectra of th Sun and Arcturus.

Wavelength [Å]	$\chi_{\rm exc}$ [eV]	$\log gf$	$\Gamma_{\rm rad}$ [rad s^{-1}]	van der Waal	Atomic/ionic species	New $\log gf$ values
15 315.660	6.280	–1.170	1.00E+05	A	Fe I	
15 320.084	4.770	–2.307	4.69E+07	A	Ti I	
15 320.897	7.030	–2.080	1.00E+05	A	Si I	
15 321.336	4.771	–3.236	4.66E+07	A	Ti I	
15 322.423	5.456	–3.487	1.85E+08	2.50	V I	
15 322.705	6.554	–1.037	8.11E+07	2.50	Co I	
15 322.752	5.923	–1.428	2.44E+08	2.50	Cr I	
15 323.287	5.206	–0.950	6.82E+07	A	Ti I	
15 323.550	6.350	–0.99	1.00E+05	A	Fe I	*
15 323.809	6.730	–3.652	4.09E+08	A	Fe II	
15 323.973	6.412	–3.406	4.12E+07	A	Mn I	
15 324.020	6.127	–2.719	8.79E+07	A	Mn I	
15 325.641	4.650	–3.349	1.07E+08	2.50	V I	
15 326.816	5.364	–2.886	7.38E+07	A	V I	
15 327.159	5.221	–3.407	6.19E+07	A	Ti I	
15 327.168	6.412	–3.018	4.34E+07	A	Mn I	
15 327.518	7.125	–2.980	1.00E+05	A	Si I	
15 327.948	3.403	–3.070	1.00E+05	A	K I	
15 328.033	2.845	–6.324	1.96E+07	A	Fe I	
15 329.048	4.851	–0.673	1.25E+08	A	V I	
15 329.166	5.541	–2.238	1.11E+08	2.50	V I	
15 329.358	3.403	–3.370	1.00E+05	A	K I	
15 329.989	5.940	–2.997	1.60E+08	A	Co I	
15 330.017	4.396	–3.084	1.10E+08	A	Ti I	
15 330.191	6.718	–1.90	1.00E+05	A	Si I	*
15 331.188	4.865	–0.265	1.39E+08	2.50	V I	
15 331.305	3.933	–3.606	2.81E+08	A	V I	
15 331.775	4.585	–1.942	6.40E+07	2.50	V I	
15 331.832	2.609	–6.538	1.46E+07	A	Fe I	
15 332.010	6.725	–3.822	2.53E+08	A	Fe I	
15 332.754	2.588	–6.292	1.50E+07	A	Fe I	
15 333.304	7.381	–0.052	4.20E+08	A	Sc II	
15 334.762	5.377	–8.655	2.70E+08	A	Mn II	
15 334.840	1.887	–1.35	2.93E+06	A	Ti I	*
15 335.011	5.607	–2.997	1.50E+08	A	Fe I	
15 335.380	5.410	0.00	1.12E+08	A	Fe I	*
15 335.456	5.270	–3.180	2.64E+08	A	Ti I	
15 335.992	5.363	–2.515	6.75E+08	A	Ni I	
15 336.315	6.546	–3.043	1.15E+08	2.50	Co I	
15 336.338	4.865	–1.200	1.39E+08	A	V I	
15 336.456	5.902	–3.140	7.91E+07	A	Fe I	
15 337.470	5.233	–2.348	2.06E+08	A	Ti I	
15 337.724	4.506	–2.804	1.80E+08	A	Ti I	
15 338.762	5.252	–3.832	9.53E+07	2.50	V I	
15 338.780	6.261	–2.580	1.00E+05	A	Si I	
15 339.000	5.233	–1.523	2.03E+08	A	Ti I	
15 339.200	5.288	–3.155	1.53E+08	A	Ni I	
15 340.153	5.494	–3.391	4.89E+08	A	Ni I	
15 341.822	5.726	–2.682	2.22E+08	A	Co I	
15 342.140	4.256	–1.299	1.85E+08	A	Ti I	
15 342.199	5.851	–3.552	2.25E+08	A	Cr I	
15 342.973	7.108	–1.85	1.00E+05	A	Si I	*
15 343.070	9.330	–3.900	1.00E+05	A	C I	
15 343.359	5.648	–3.534	1.29E+08	A	Fe I	
15 343.494	5.529	–2.239	2.23E+08	A	Sc I	
15 343.810	5.653	–0.70	1.16E+08	A	Fe I	*
15 344.883	4.586	–1.470	6.52E+07	2.50	V I	
15 345.010	5.478	–2.010	1.79E+08	A	Fe I	
15 345.307	5.289	–4.043	1.38E+08	A	Ni I	
15 345.425	8.086	–0.934	4.70E+08	A	Ti II	

Table 7. continued.

Wavelength [Å]	χ_{exc} [eV]	log gf	Γ_{rad} [rad s^{-1}]	van der Waal	Atomic/ionic species	New log gf values
15 345.802	7.424	–0.759	4.08E+08	A	Sc II	
15 345.920	6.270	–1.190	1.00E+05	A	Fe I	
15 346.132	9.331	–3.020	1.00E+05	A	C I	
15 346.827	4.850	–3.648	1.85E+08	A	Ti I	
15 348.252	5.464	–1.785	8.22E+07	2.50	V I	
15 348.398	5.874	–1.70	9.18E+07	A	Fe I	*
15 348.723	4.835	–3.379	2.06E+08	A	Fe I	
15 348.904	3.397	–1.070	1.00E+05	A	K I	
15 348.904	3.397	–2.380	1.00E+05	A	K I	
15 348.950	5.950	–1.00	1.00E+05	A	Fe I	*
15 348.950	7.010	–1.210	1.00E+05	A	Mn I	
15 350.491	3.791	–1.554	3.20E+08	A	Sc I	
15 351.426	3.397	–1.230	1.00E+05	A	K I	
15 352.410	5.458	–3.227	1.20E+08	A	Fe I	
15 352.612	5.059	–2.307	7.03E+07	A	Sc I	
15 352.919	5.377	–7.823	2.70E+08	A	Mn II	
15 353.155	8.098	–1.983	4.74E+08	A	Ti II	
15 354.098	4.598	–2.165	1.43E+08	A	Sc I	
15 354.756	6.223	–4.020	1.00E+05	A	Si I	
15 355.230	5.925	–1.832	2.46E+08	2.50	Cr I	
15 355.513	4.725	–3.070	1.46E+08	A	V I	
15 355.560	4.712	–2.525	1.39E+08	A	V I	
15 356.221	3.010	–4.271	6.64E+06	A	Cr I	
15 356.928	4.656	–2.931	1.43E+08	A	V I	
15 357.046	4.652	–3.345	2.61E+08	A	V I	
15 357.683	4.889	–1.988	1.71E+08	A	Mn I	
15 358.238	6.150	–3.741	1.06E+08	A	Fe I	
15 358.351	6.361	–2.680	2.28E+08	A	Fe I	
15 359.618	5.436	–3.597	1.63E+08	2.50	V I	
15 359.722	5.228	–7.048	5.79E+07	A	Ca I	
15 359.736	3.799	–5.272	2.84E+08	A	V II	
15 359.901	5.925	–1.733	2.27E+08	2.50	Cr I	
15 359.915	7.064	–1.950	1.00E+05	A	Si I	
15 360.019	6.127	–2.457	8.79E+07	A	Mn I	
15 360.230	4.260	–2.97	8.75E+06	A	Fe I	*
15 360.534	5.229	–5.890	5.78E+07	A	Ca I	
15 361.160	5.954	–2.12	1.00E+05	A	Si I	*
15 361.742	4.078	–2.142	7.10E+07	A	V I	
15 362.049	4.888	–3.677	1.08E+08	A	Sc I	
15 363.045	5.026	–4.761	1.99E+07	A	Ca I	
15 363.890	6.022	–3.993	4.71E+08	2.50	Co I	
15 364.174	4.967	–2.348	1.05E+08	A	Sc I	
15 364.415	5.253	–2.773	4.63E+07	A	Ti I	
15 364.599	5.462	–2.431	2.47E+08	A	Cr I	
15 365.732	6.006	–2.150	3.66E+08	A	Co I	
15 365.874	5.330	–7.100	2.63E+08	A	Cr II	
15 365.968	5.812	–3.902	2.64E+08	A	Cr I	
15 366.521	5.228	–6.343	5.52E+07	A	Ca I	
15 366.677	5.936	–3.223	7.35E+07	2.50	Cr I	
15 367.334	5.229	–4.789	5.51E+07	A	Ca I	
15 367.560	5.228	–4.827	5.52E+07	A	Ca I	
15 367.740	4.922	–0.545	9.10E+07	A	Sc I	
15 368.104	5.228	–4.111	5.52E+07	A	Ca I	
15 368.373	5.229	–3.916	5.51E+07	A	Ca I	
15 368.439	5.229	–3.712	5.51E+07	A	Ca I	
15 369.684	5.814	–3.556	1.44E+08	A	Fe I	
15 370.953	8.089	–0.255	4.83E+08	A	Ti II	
15 371.320	5.870	–2.240	1.00E+05	A	Fe I	
15 371.430	5.303	–3.310	1.29E+08	A	Ni I	
15 371.473	4.498	–1.122	6.10E+07	A	Sc I	
15 371.590	5.303	–2.430	1.29E+08	A	Ni I	
15 371.750	5.303	–2.010	1.29E+08	A	Ni I	
15 372.702	4.059	–2.259	2.72E+08	A	V I	
15 372.986	6.006	–1.829	3.24E+08	A	Co I	

Table 7. continued.

Wavelength [Å]	χ_{exc} [eV]	log gf	Γ_{rad} [rad s^{-1}]	van der Waal	Atomic/ionic species	New log gf values
15 374.256	5.125	–2.571	1.19E+08	A	Ti I	
15 374.263	6.212	–2.826	3.57E+08	2.50	Mn I	
15 375.340	5.920	–1.870	1.00E+05	A	Fe I	
15 375.412	5.026	–2.856	2.01E+07	A	Ca I	
15 375.430	6.734	–1.530	1.00E+05	A	Si I	
15 375.440	5.202	–3.635	1.50E+08	A	Ti I	
15 376.249	5.948	–1.826	1.55E+08	2.50	Cr I	
15 376.348	5.502	–3.360	1.54E+08	A	Fe I	
15 376.500	4.733	–4.085	2.07E+08	A	Fe I	
15 376.830	6.223	–0.61	1.00E+05	A	Si I	*
15 376.830	6.721	–1.08	1.00E+05	A	Si I	*
15 376.888	4.579	–2.950	1.86E+08	A	Sc I	
15 378.614	3.011	–3.962	6.64E+06	A	Cr I	
15 378.676	5.280	–2.524	1.34E+08	A	Ni I	
15 379.040	6.280	–3.236	1.91E+08	A	Fe I	
15 379.296	5.446	–3.287	2.29E+08	A	Fe I	
15 379.513	4.929	–1.175	1.22E+08	A	Sc I	
15 379.750	8.116	–1.403	4.78E+08	A	Ti II	
15 380.117	5.481	–2.113	2.13E+08	A	Ni I	
15 381.044	5.203	–2.856	3.35E+08	A	Ti I	
15 381.080	5.230	–2.645	8.02E+07	A	Ti I	
15 381.110	2.333	–2.29	7.13E+07	A	Ti I	*
15 381.217	3.640	–6.217	9.86E+07	A	Fe I	
15 381.288	8.114	–0.396	5.08E+08	A	Ti II	
15 381.738	6.721	–2.030	1.00E+05	A	Si I	
15 381.980	3.640	–3.03	1.00E+05	A	Fe I	*
15 382.753	2.305	–6.848	1.73E+06	A	Ti I	
15 382.992	7.951	–2.741	6.10E+08	A	V II	
15 384.110	6.200	–1.460	1.00E+05	A	Fe I	
15 387.069	7.166	–1.640	1.00E+05	A	Si I	
15 387.635	4.769	–5.281	1.58E+08	A	Ca I	
15 387.800	6.280	–0.270	1.00E+05	A	Fe I	
15 388.746	4.650	–2.411	1.51E+09	A	V I	
15 388.976	5.140	–3.602	1.15E+08	A	Ti I	
15 389.819	5.219	–0.859	7.11E+07	A	Ti I	
15 390.028	5.497	–3.477	3.29E+08	A	Ni I	
15 390.428	4.579	–1.511	1.85E+08	A	Sc I	
15 390.663	5.853	–1.302	3.54E+08	A	Ni I	
15 390.826	4.669	–0.777	1.19E+08	A	Ti I	
15 390.902	8.599	–2.858	6.17E+08	A	V II	
15 391.281	4.975	–1.837	7.48E+07	2.50	Sc I	
15 391.968	5.161	–2.020	1.18E+08	A	Ti I	
15 394.670	5.621	–0.03	1.61E+08	A	Fe I	*
15 394.680	2.469	–9.023	5.82E+03	A	Fe I	
15 394.777	5.045	–1.729	4.20E+07	A	Ca I	
15 395.720	5.621	–0.23	1.21E+08	A	Fe I	*
15 396.093	5.122	–3.938	3.70E+08	A	Co II	
15 397.357	4.769	–5.386	1.58E+08	A	Ca I	
15 397.629	4.398	–2.926	1.19E+07	A	Ti I	
15 397.753	4.885	–1.264	1.36E+08	A	V I	
15 399.285	2.334	–2.130	7.13E+07	A	Ti I	
15 399.605	5.621	–3.216	1.21E+08	A	Fe I	
15 399.989	4.515	–2.449	1.83E+08	A	Ti I	
15 400.060	8.700	0.100	1.00E+05	A	S I	
15 400.082	8.307	–3.765	4.98E+08	A	Fe II	
15 401.833	6.728	–3.525	2.53E+08	A	Fe I	
15 402.065	4.769	–5.265	1.58E+08	A	Ca I	
15 402.331	7.439	–2.555	3.99E+08	A	Sc II	
15 402.331	8.699	–1.60	1.00E+05	A	S I	*
15 403.072	4.770	–2.457	7.53E+07	A	Ti I	
15 403.494	8.071	–0.300	4.89E+08	A	Ti II	
15 403.770	8.700	0.35	1.00E+05	A	S I	*
15 403.921	5.011	–9.415	2.50E+08	A	Cr II	
15 404.206	4.638	–3.270	2.62E+08	A	V I	
15 405.191	5.214	–2.857	1.35E+08	A	Ti I	
15 405.227	3.823	–4.374	4.06E+07	A	V I	

Table 7. continued.

Wavelength [Å]	χ_{exc} [eV]	log gf	Γ_{rad} [rad s^{-1}]	van der Waal	Atomic/ionic species	New log gf values
15 405.227	4.664	–1.567	1.50E+08	A	V I	
15 405.979	8.700	–1.50	1.00E+05	A	S I	*
15 406.485	2.950	–1.121	1.00E+05	A	Rb I	
15 406.699	5.700	–3.446	3.09E+08	A	Co I	
15 406.865	5.464	–0.996	2.47E+08	A	Cr I	
15 407.048	5.967	–3.607	1.63E+08	A	Fe I	
15 407.079	5.062	–1.002	6.98E+07	A	Sc I	
15 407.143	5.614	–3.761	1.40E+08	A	Fe I	
15 407.435	5.521	–2.728	1.02E+08	2.50	V I	
15 408.560	5.648	–2.290	1.51E+08	A	Fe I	
15 408.864	5.283	–2.953	1.52E+08	A	Ti I	
15 409.335	8.583	–3.623	6.41E+08	A	V II	
15 410.071	2.950	–2.075	1.00E+05	A	Rb I	
15 410.261	3.013	–4.442	6.64E+06	A	Cr I	
15 411.513	5.250	–6.097	1.13E+08	A	Ca I	
15 411.627	5.519	–3.159	1.69E+08	A	Fe I	
15 412.254	6.726	–2.60	1.00E+05	A	Mg I	*
15 412.748	5.250	–3.896	1.13E+08	A	Ca I	
15 415.289	6.726	–1.870	1.00E+05	A	Mg I	
15 415.289	6.726	–2.15	1.00E+05	A	Mg I	*
15 415.346	5.445	–1.693	4.42E+08	2.50	V I	
15 415.850	5.980	–2.100	1.00E+05	A	Fe I	
15 415.917	4.650	–0.189	8.99E+07	2.50	V I	
15 415.964	4.925	–1.971	6.52E+07	A	Sc I	
15 416.428	5.538	–2.999	2.74E+08	A	Fe I	
15 416.485	5.538	–3.207	2.89E+08	A	Fe I	
15 416.589	4.771	–2.058	7.53E+07	A	Ti I	
15 416.965	3.642	–7.769	9.86E+07	A	Fe I	
15 417.231	4.424	–1.232	1.02E+08	A	Ti I	
15 417.578	5.607	–4.078	1.32E+08	A	Fe I	
15 418.294	5.541	–2.888	1.01E+08	2.50	V I	
15 418.461	4.706	–2.005	2.55E+08	A	V I	
15 418.865	5.855	–3.478	2.43E+08	A	Cr I	
15 419.079	1.804	–3.958	1.09E+07	A	V I	
15 419.643	5.250	–0.779	1.26E+08	A	Ca I	
15 420.649	5.089	–2.600	6.41E+07	A	Co I	
15 420.806	7.006	–2.33	1.00E+05	1.30	Si I	*
15 420.884	5.502	–3.442	2.45E+08	A	Fe I	
15 421.567	6.727	–1.70	1.00E+05	A	Mg I	*
15 421.567	6.727	–1.790	1.00E+05	A	Mg I	
15 421.567	6.727	–3.340	1.00E+05	A	Mg I	
15 421.662	7.006	–2.660	1.00E+05	1.30	Si I	
15 422.076	8.056	–0.554	4.95E+08	A	Ti II	
15 422.260	8.701	0.55	1.00E+05	A	S I	*
15 422.260	8.701	–0.620	1.00E+05	A	S I	
15 422.680	6.340	–0.910	1.00E+05	A	Fe I	
15 422.980	5.599	–3.876	1.73E+08	A	Mn I	
15 424.455	7.772	–4.602	2.88E+08	A	Cr II	
15 424.455	8.701	–1.920	1.00E+05	A	S I	
15 425.348	5.188	–2.554	2.64E+08	A	Ti I	
15 426.520	6.160	–2.860	1.00E+05	A	Fe I	
15 426.970	1.873	–2.52	2.76E+06	A	Ti I	*
15 427.097	5.782	–2.530	1.23E+08	A	Cr I	
15 427.407	7.757	–5.217	3.08E+08	A	Mn II	
15 427.610	6.450	–0.980	1.00E+05	A	Fe I	
15 428.478	4.597	–1.034	8.17E+07	2.50	V I	
15 430.050	5.140	–2.556	1.19E+08	A	Ti I	
15 431.450	7.134	–3.590	1.00E+05	A	Si I	
15 431.650	6.261	–3.720	1.00E+05	A	Si I	
15 431.955	6.201	–0.771	2.62E+08	A	Mn I	
15 432.453	4.854	–2.753	1.85E+08	A	Ti I	
15 434.409	5.856	–2.675	2.31E+08	A	Cr I	
15 434.433	5.570	–3.485	9.82E+07	2.50	V I	
15 434.981	5.855	–3.045	2.31E+08	A	Co I	
15 435.360	7.125	–2.240	1.00E+05	A	Si I	

Table 7. continued.

Wavelength [Å]	χ_{exc} [eV]	log gf	Γ_{rad} [rad s^{-1}]	van der Waal	Atomic/ionic species	New log gf values
15 436.261	5.900	–2.611	1.27E+08	A	Fe I	
15 437.320	5.840	–1.910	1.00E+05	A	Fe I	
15 437.467	4.607	–4.030	2.62E+08	A	Fe I	
15 437.477	5.839	–2.552	1.29E+08	A	Fe I	
15 438.135	2.740	–5.022	3.00E+05	A	Ni I	
15 438.194	4.411	–1.972	2.17E+08	A	Ti I	
15 438.480	1.502	–4.626	1.69E+06	A	Ti I	
15 440.047	2.305	–7.337	1.72E+06	A	Ti I	
15 440.354	5.943	–3.227	1.35E+08	A	Fe I	
15 441.177	6.552	–1.510	1.00E+05	A	Cu I	
15 441.418	4.777	–3.611	3.92E+07	A	Ti I	
15 441.800	5.874	–1.840	1.09E+08	A	Fe I	
15 441.957	3.415	–5.436	1.65E+08	A	Fe I	
15 442.682	5.526	–3.960	3.89E+08	A	Co I	
15 443.517	4.063	–4.145	6.68E+07	A	V I	
15 444.185	5.464	–1.353	5.02E+08	2.50	V I	
15 445.283	7.758	–4.023	3.08E+08	A	Mn II	
15 445.381	5.614	–3.546	1.38E+08	A	Fe I	
15 445.855	4.978	–2.553	1.02E+08	2.50	Sc I	
15 447.526	4.603	–2.074	1.44E+08	A	Sc I	
15 447.836	4.627	–3.415	2.57E+08	A	V I	
15 448.352	5.481	–3.263	2.15E+08	A	Ni I	
15 450.869	6.125	–1.758	1.53E+08	A	Ni I	
15 451.330	6.450	–0.48	1.00E+05	A	Fe I	*
15 451.940	6.290	–1.290	1.00E+05	A	Fe I	
15 451.940	6.340	–1.290	1.00E+05	A	Fe I	
15 452.755	5.234	–2.386	1.04E+08	A	Ti I	
15 453.080	7.069	–3.120	1.00E+05	A	Si I	
15 453.343	3.867	–1.915	6.49E+07	A	Ti I	
15 454.045	5.036	–4.005	1.21E+08	A	Co I	
15 454.356	6.212	–0.772	2.51E+08	A	Mn I	
15 454.456	5.283	–2.732	1.36E+08	A	Ti I	
15 456.028	6.185	–1.124	2.86E+08	A	Mn I	
15 456.270	6.340	–1.790	1.00E+05	A	Fe I	
15 456.666	2.450	–9.207	7.83E+03	A	Fe I	
15 456.728	5.648	–3.730	1.30E+08	A	Fe I	
15 456.733	5.913	–2.697	1.29E+08	A	Fe I	
15 459.398	4.049	–3.275	7.10E+07	A	V I	
15 461.191	5.510	–3.356	1.26E+08	2.50	V I	
15 461.220	4.186	–4.341	3.97E+08	A	Fe I	
15 462.267	5.978	–2.418	3.52E+08	A	Co I	
15 462.420	6.290	–2.070	1.00E+05	A	Fe I	
15 462.650	5.941	–2.394	9.33E+07	2.50	Cr I	
15 463.033	5.537	–4.067	3.48E+08	A	V II	
15 463.710	5.284	–1.640	4.29E+08	A	Ni I	
15 464.820	5.049	–1.620	7.96E+07	A	Ca I	
15 466.023	6.412	–2.174	6.37E+07	A	Mn I	
15 466.645	9.007	–1.869	2.89E+08	A	Mn II	
15 466.813	5.464	–1.141	9.59E+07	2.50	V I	
15 467.729	4.640	–0.164	8.83E+07	A	V I	
15 467.985	6.028	–3.920	4.02E+08	2.50	Co I	
15 468.122	4.396	–3.628	2.00E+08	A	Ti I	
15 468.655	6.212	–2.323	3.44E+08	2.50	Mn I	
15 469.820	8.045	–0.45	1.00E+05	A	S I	*
15 470.293	6.803	–4.600	3.07E+08	A	Fe II	
15 470.570	4.394	–3.525	2.87E+08	A	Ti I	
15 471.121	5.953	–1.627	2.55E+08	2.50	Cr I	
15 471.964	6.726	–2.40	1.00E+05	A	Si I	*
15 472.098	4.355	–3.052	2.21E+08	A	Ti I	
15 472.701	6.006	–3.184	3.14E+08	A	Co I	
15 473.252	4.644	–3.500	1.02E+08	A	V I	
15 473.324	5.760	–3.340	2.01E+08	A	Co I	
15 474.603	5.902	–3.659	1.39E+08	A	Fe I	
15 474.641	5.480	–3.149	3.50E+08	A	V II	
15 474.977	7.430	–1.194	4.05E+08	A	Sc II	
15 475.190	5.486	–2.110	1.36E+08	A	Fe I	

Table 7. continued.

Wavelength [Å]	χ_{exc} [eV]	log gf	Γ_{rad} [rad s^{-1}]	van der Waal	Atomic/ionic species	New log gf values
15 475.190	6.310	–0.730	1.00E+05	A	Fe I	
15 475.620	8.046	–0.890	1.00E+05	A	S I	
15 475.808	3.967	–9.036	2.94E+08	A	Fe II	
15 475.887	4.585	–1.706	7.29E+07	2.50	V I	
15 475.923	5.874	–2.00	1.26E+08	A	Fe I	*
15 476.500	6.320	–1.140	1.00E+05	A	Fe I	
15 476.917	4.690	–0.055	1.39E+08	A	Ti I	
15 478.480	8.046	–0.220	1.00E+05	A	S I	
15 478.870	6.240	–0.600	1.00E+05	A	Fe I	
15 478.978	4.741	–3.181	1.32E+08	A	V I	
15 479.050	6.101	–3.075	2.66E+08	A	V II	
15 479.600	6.320	–1.120	1.00E+05	A	Fe I	
15 480.081	4.232	–3.345	1.02E+08	A	V I	
15 480.230	5.614	–2.270	1.56E+08	A	Fe I	
15 480.967	2.328	–8.788	1.96E+04	A	Co I	
15 481.087	7.439	–1.140	4.02E+08	A	Sc II	
15 481.878	7.760	–3.150	3.08E+08	A	Mn II	
15 481.936	4.433	–1.610	2.00E+08	A	Ti I	
15 484.420	4.650	–0.948	9.04E+07	2.50	V I	
15 484.495	6.582	–2.973	5.66E+07	A	Fe I	
15 485.450	6.280	–0.93	1.00E+05	A	Fe I	*
15 485.452	5.140	–3.360	1.19E+08	A	Ti I	
15 486.627	4.168	–2.265	2.04E+08	A	Sc I	
15 487.097	5.241	–3.031	7.69E+07	A	Ti I	
15 488.590	5.928	–3.431	1.04E+08	A	Fe I	
15 488.657	5.241	–3.578	7.40E+07	A	Ti I	
15 488.813	7.104	–2.50	1.00E+05	A	Si I	*
15 489.425	5.181	–2.749	5.61E+07	A	Ca I	
15 489.458	6.421	–1.935	4.12E+07	A	Mn I	
15 489.626	4.967	–1.708	1.06E+08	A	Sc I	
15 489.658	4.420	–2.739	1.54E+08	A	Ti I	
15 489.674	6.054	–3.104	1.66E+08	A	Co I	
15 489.960	5.879	–3.509	1.77E+08	A	Fe I	
15 489.986	8.093	–1.216	4.69E+08	A	Ti II	
15 490.073	3.869	–2.881	6.67E+07	A	Ti I	
15 490.340	2.198	–4.85	1.14E+04	1.40	Fe I	*
15 490.490	5.319	–6.527	2.35E+08	A	Cr II	
15 490.880	6.290	–0.57	1.00E+05	A	Fe I	*
15 490.971	7.832	–1.551	1.21E+09	A	Ti II	
15 492.140	5.839	–1.950	1.27E+08	A	Fe I	
15 493.515	6.368	–1.45	2.34E+08	A	Fe I	*
15 493.550	6.450	–1.25	1.00E+05	A	Fe I	*
15 494.800	5.177	–3.163	3.30E+08	A	Ti I	
15 495.244	7.472	–2.980	4.50E+08	A	Sc II	
15 495.364	4.929	–2.838	1.18E+08	A	Sc I	
15 495.456	5.168	–2.201	9.59E+07	A	Ca I	
15 495.667	7.006	–3.110	1.00E+05	1.30	Si I	
15 496.690	6.290	–0.300	1.00E+05	A	Fe I	
15 496.830	5.102	–2.286	7.74E+07	2.50	Sc I	
15 496.964	7.006	–2.54	1.00E+05	1.30	Si I	*
15 497.000	6.269	–3.400	1.00E+05	A	Si I	
15 497.040	6.290	–1.140	1.00E+05	A	Fe I	
15 499.232	5.506	–3.100	2.30E+08	A	Fe I	
15 499.410	6.350	–0.32	1.00E+05	A	Fe I	*
15 499.689	5.796	–2.975	2.25E+08	A	Co I	
15 500.073	4.504	–0.244	5.75E+07	A	Sc I	
15 500.241	9.036	–3.901	8.30E+08	A	V II	
15 500.316	4.361	–2.823	8.11E+07	A	Ti I	
15 500.650	6.201	–1.332	3.12E+08	2.50	Mn I	
15 500.800	6.320	–0.12	1.00E+05	A	Fe I	*
15 501.080	5.943	–3.981	1.92E+08	A	Fe I	
15 501.320	6.290	0.10	1.00E+05	A	Fe I	*
15 502.170	6.350	–1.070	1.00E+05	A	Fe I	
15 502.429	3.409	–4.954	1.46E+08	A	Co I	
15 502.640	7.134	–1.870	1.00E+05	A	Si I	

Table 7. continued.

Wavelength [Å]	χ_{exc} [eV]	log gf	Γ_{rad} [rad s^{-1}]	van der Waal	Atomic/ionic species	New log gf values
15 503.246	3.375	–4.682	5.86E+06	A	Cr I	
15 503.246	4.168	–1.810	2.14E+08	A	Sc I	
15 503.840	5.972	–3.183	3.33E+08	A	Fe I	
15 503.943	5.726	–3.178	2.24E+08	A	Co I	
15 503.967	4.725	–2.564	1.05E+08	A	V I	
15 505.771	4.389	–2.911	1.22E+07	A	Ti I	
15 506.105	5.524	–3.367	1.67E+08	A	Fe I	
15 506.252	4.968	–2.486	9.68E+07	A	Sc I	
15 506.980	6.727	–1.80	1.00E+05	A	Si I	*
15 507.022	4.865	–0.479	1.44E+08	A	V I	
15 507.043	8.228	–1.500	1.00E+05	A	P I	
15 507.103	4.770	–2.115	4.91E+07	A	Ti I	
15 507.118	8.943	–3.497	3.84E+08	A	Fe II	
15 507.623	5.235	–0.895	6.70E+07	A	Ti I	
15 508.385	4.771	–3.338	4.89E+07	A	Ti I	
15 511.117	7.166	–2.850	1.00E+05	A	Si I	
15 511.528	5.476	–3.146	2.28E+08	A	Fe I	
15 512.724	4.681	–1.408	8.93E+07	2.50	V I	
15 513.511	4.515	–2.559	1.81E+08	A	Ti I	
15 514.280	6.290	–0.750	1.00E+05	A	Fe I	
15 514.691	7.092	–2.270	1.00E+05	A	Si I	
15 515.368	2.305	–4.104	1.72E+06	A	Ti I	
15 515.373	4.646	–2.758	1.10E+08	A	V I	
15 515.760	6.290	–1.700	1.00E+05	A	Fe I	
15 515.876	4.793	–2.070	2.27E+08	A	Ti I	
15 516.720	6.290	–1.330	1.00E+05	A	Fe I	
15 517.275	5.744	–3.579	3.07E+08	A	Co I	
15 518.720	5.104	–0.756	7.76E+07	2.50	Sc I	
15 518.900	6.280	–1.380	1.00E+05	A	Fe I	
15 519.100	6.290	–1.160	1.00E+05	A	Fe I	
15 519.360	6.290	–0.570	1.00E+05	A	Fe I	
15 519.636	4.111	–1.236	3.13E+08	A	V I	
15 519.942	2.484	–5.827	1.40E+07	A	Fe I	
15 519.949	3.807	–1.148	3.16E+08	A	Sc I	
15 520.115	7.108	–1.85	1.00E+05	A	Si I	*
15 521.086	5.352	–3.473	1.98E+08	A	Fe I	
15 521.690	6.320	–1.440	1.00E+05	A	Fe I	
15 522.600	6.212	–2.760	1.07E+08	A	Co I	
15 522.640	6.320	–0.97	1.00E+05	A	Fe I	*
15 523.998	6.054	–3.914	1.78E+08	A	Co I	
15 524.277	2.740	–7.135	4.63E+04	A	Ni I	
15 524.300	5.790	–1.510	1.00E+05	A	Fe I	
15 524.543	5.793	–2.15	2.55E+08	A	Fe I	*
15 525.227	5.840	–2.738	1.17E+08	A	Fe I	
15 525.661	4.885	–0.054	1.63E+08	2.50	V I	
15 525.734	8.097	–0.400	5.12E+08	A	Ti II	
15 525.738	4.793	–1.559	2.27E+08	A	Ti I	
15 527.210	6.320	–1.010	1.00E+05	A	Fe I	
15 527.535	7.140	–3.220	1.00E+05	A	Si I	
15 528.109	5.947	–2.974	4.53E+08	A	Fe I	
15 530.043	3.573	–6.583	9.31E+07	A	Fe I	
15 530.195	5.445	–1.530	8.15E+07	2.50	V I	
15 531.288	4.654	–0.201	1.93E+08	A	Ti I	
15 531.750	5.642	–0.48	1.22E+08	A	Fe I	*
15 532.263	7.140	–2.450	1.00E+05	A	Si I	
15 532.449	6.718	–2.18	1.00E+05	A	Si I	*
15 533.977	7.140	–3.660	1.00E+05	A	Si I	
15 534.260	5.642	–0.30	1.21E+08	A	Fe I	*
15 537.450	5.790	–1.710	1.00E+05	A	Fe I	
15 537.572	5.793	–1.410	2.56E+08	A	Fe I	
15 537.690	6.320	–0.50	1.71E+08	A	Fe I	*
15 538.064	5.744	–1.809	3.21E+08	A	Co I	
15 538.463	6.761	–2.36	1.00E+05	A	Si I	*
15 539.417	5.957	–4.069	6.44E+07	2.50	Cr I	
15 541.547	5.844	–3.014	2.15E+08	A	Fe I	
15 541.852	5.967	–2.837	2.25E+08	A	Fe I	

Table 7. continued.

Wavelength [Å]	χ_{exc} [eV]	log gf	Γ_{rad} [rad s^{-1}]	van der Waal	Atomic/ionic species	New log gf values
15 541.857	6.371	–1.868	1.93E+08	A	Fe I	
15 542.016	7.006	–1.380	1.00E+05	1.30	Si I	
15 542.090	5.642	–0.700	1.64E+08	A	Fe I	
15 542.090	7.010	–1.380	1.00E+05	A	Si I	
15 542.197	4.690	–0.726	1.17E+08	A	Ti I	
15 542.731	4.394	–3.457	2.79E+08	A	Ti I	
15 543.357	4.860	–1.938	1.85E+08	A	Ti I	
15 543.780	1.879	–1.45	2.76E+06	A	Ti I	*
15 543.838	4.795	–1.310	2.40E+08	A	Ti I	
15 544.152	6.792	–1.440	1.00E+05	A	Cu I	
15 544.355	2.487	–7.407	7.66E+07	A	Ti I	
15 546.081	4.405	–1.930	2.26E+08	A	Ti I	
15 548.978	5.181	–6.986	5.38E+07	A	Ca I	
15 550.450	6.340	–0.340	1.71E+08	A	Fe I	
15 550.560	6.112	–3.186	6.25E+07	A	Fe I	
15 551.430	6.350	–0.290	1.71E+08	A	Fe I	
15 551.818	4.664	–2.093	1.65E+08	A	V I	
15 552.108	8.108	–1.104	4.71E+08	A	Ti II	
15 552.222	5.621	–4.20	1.09E+08	A	Fe I	*
15 553.245	5.537	–4.569	2.27E+08	A	V II	
15 553.560	5.478	–3.056	2.65E+08	A	Fe I	
15 554.510	6.280	–1.20	1.00E+05	A	Fe I	*
15 554.510	6.410	–1.240	1.00E+05	A	Fe I	
15 554.557	4.433	–1.828	1.76E+08	A	Ti I	
15 554.625	4.607	–3.570	9.79E+07	2.50	V I	
15 554.697	5.868	–3.799	3.67E+08	A	V II	
15 555.120	5.280	–0.610	1.00E+05	A	Ni I	
15 555.210	5.280	–1.030	1.00E+05	A	Ni I	
15 555.370	5.488	0.08	1.48E+08	A	Ni I	*
15 555.641	5.059	–1.139	7.35E+07	A	Sc I	
15 556.016	5.283	–3.15	1.68E+08	A	Ni I	*
15 556.122	6.552	–1.320	1.00E+05	A	Cu I	
15 556.670	5.930	–2.804	1.38E+08	A	Fe I	
15 556.711	5.297	–2.788	1.55E+08	A	Ti I	
15 557.602	4.681	–4.320	1.80E+08	A	V I	
15 557.689	5.289	–2.010	8.97E+07	A	Ti I	
15 557.790	5.964	–0.62	1.00E+05	A	Si I	*
15 558.585	4.500	–2.580	2.05E+08	A	Ti I	
15 559.500	5.868	–2.459	1.24E+08	A	Ni I	
15 559.849	5.928	–3.843	1.04E+08	A	Fe I	
15 559.922	5.168	–6.944	9.06E+07	A	Ca I	
15 560.780	6.350	–0.510	1.00E+05	A	Fe I	
15 561.041	6.078	–4.003	2.57E+08	A	Co I	
15 561.251	7.040	–1.380	1.00E+05	A	Si I	
15 561.268	6.711	–3.630	4.45E+08	A	Fe I	
15 562.080	4.627	–4.159	5.87E+07	A	V I	
15 562.300	6.366	–2.677	1.81E+08	A	Ni I	
15 563.463	5.237	–3.380	5.13E+07	A	Cr I	
15 564.020	9.053	–3.801	8.38E+08	A	Fe II	
15 564.369	5.614	–2.378	1.38E+08	A	Fe I	
15 564.723	4.527	–2.044	3.28E+07	A	Sc I	
15 565.230	6.320	–0.950	1.00E+05	A	Fe I	
15 565.886	4.640	–0.903	9.82E+07	2.50	V I	
15 566.725	6.350	–0.53	1.71E+08	A	Fe I	*
15 567.001	4.967	–1.920	1.07E+08	A	Sc I	
15 567.188	7.113	–3.830	1.00E+05	1.30	Si I	
15 567.261	6.350	–3.891	1.71E+08	A	Fe I	
15 567.680	4.623	–3.966	2.27E+08	A	V I	
15 567.728	4.586	–3.805	1.10E+08	2.50	V I	
15 568.187	7.108	–4.270	1.00E+05	A	Si I	
15 568.325	5.883	–2.447	1.14E+08	A	Fe I	
15 568.383	4.667	–3.512	1.49E+08	A	V I	
15 569.103	7.113	–3.470	1.00E+05	1.30	Si I	
15 569.240	5.512	–2.360	1.48E+08	A	Fe I	
15 569.741	5.750	–1.122	1.43E+08	A	Co I	

Table 7. continued.

Wavelength [Å]	χ_{exc} [eV]	log gf	Γ_{rad} [rad s^{-1}]	van der Waal	Atomic/ionic species	New log gf values
15 570.202	8.416	–2.469	4.69E+08	A	Ni II	
15 571.099	4.681	–0.285	1.62E+08	A	V I	
15 571.120	5.879	–1.690	1.75E+08	A	Fe I	
15 571.729	2.575	–6.048	1.61E+06	A	V I	
15 571.740	6.320	–0.900	1.00E+05	A	Fe I	
15 572.166	5.541	–3.128	2.00E+08	A	Sc I	
15 572.632	4.669	–0.028	1.87E+08	A	Ti I	
15 572.651	4.649	–2.634	1.24E+08	A	V I	
15 573.976	5.936	–2.790	7.24E+07	2.50	Cr I	
15 574.060	6.310	–1.440	1.00E+05	A	Fe I	
15 576.040	5.507	–2.270	2.49E+08	A	Fe I	
15 576.528	5.169	–3.362	3.67E+08	A	Ti I	
15 577.594	5.250	–6.311	1.18E+08	A	Ca I	
15 577.861	5.250	–3.983	1.18E+08	A	Ca I	
15 579.080	6.320	–1.05	1.00E+05	A	Fe I	*
15 579.568	4.726	–1.553	2.52E+08	A	V I	
15 580.150	6.149	–1.887	1.15E+08	A	Mn I	
15 580.434	5.250	–1.210	1.54E+08	A	Ca I	
15 580.876	7.125	–2.910	1.00E+05	A	Si I	
15 582.333	4.409	–1.376	1.11E+08	A	Ti I	
15 582.987	5.796	–4.133	2.07E+08	A	Fe I	
15 583.793	4.968	–1.804	9.75E+07	A	Sc I	
15 584.619	5.021	–2.579	5.53E+07	2.50	Sc I	
15 585.360	6.360	–3.139	1.83E+08	A	Fe I	
15 585.528	6.285	–2.755	2.05E+08	A	Ni I	
15 585.785	8.098	–1.623	4.71E+08	A	Ti II	
15 587.195	5.766	–3.053	2.67E+08	A	Co I	
15 587.282	4.396	–1.528	1.23E+08	A	Ti I	
15 587.316	4.958	–1.608	6.85E+07	A	Sc I	
15 588.260	5.490	–2.70	1.00E+05	A	Fe I	*
15 588.260	6.370	0.34	1.00E+05	A	Fe I	*
15 588.626	5.491	–2.759	1.69E+08	A	Fe I	
15 588.699	6.484	–3.638	3.58E+08	A	Fe I	
15 588.947	5.447	–2.849	1.19E+08	A	Ni I	
15 589.139	4.865	–2.506	1.21E+08	2.50	V I	
15 589.455	5.140	–3.774	1.17E+08	A	Ti I	
15 589.626	5.175	–4.426	3.72E+08	A	Co II	
15 589.893	4.986	–0.988	7.60E+07	2.50	Sc I	
15 590.050	6.240	–0.430	1.00E+05	A	Fe I	
15 590.301	4.106	–2.583	1.24E+08	A	Ti I	
15 590.914	4.191	–3.859	1.78E+07	A	Sc I	
15 591.490	6.240	0.450	1.00E+05	A	Fe I	
15 591.490	6.360	0.450	1.00E+05	A	Fe I	
15 591.595	6.242	0.129	1.93E+08	A	Fe I	
15 591.717	6.045	–1.924	1.46E+08	A	Co I	
15 591.841	6.269	–3.640	1.00E+05	A	Si I	
15 592.762	4.664	–0.838	1.07E+08	2.50	V I	
15 592.859	4.954	–1.832	1.40E+08	A	Sc I	
15 592.874	4.411	–2.420	1.69E+08	A	Ti I	
15 593.149	4.382	–3.184	1.20E+07	A	Ti I	
15 593.202	5.879	–3.570	1.13E+08	A	Fe I	
15 593.718	5.026	–1.353	2.03E+07	A	Ca I	
15 593.740	5.033	–1.92	5.96E+08	A	Fe I	*
15 594.076	4.965	–2.999	3.46E+07	2.50	Sc I	
15 594.903	2.871	–6.423	1.06E+07	A	Co I	
15 595.878	4.780	–4.715	1.58E+08	A	Ca I	
15 596.114	5.796	–2.843	2.09E+08	A	Fe I	
15 596.192	4.090	–1.413	3.13E+08	A	V I	
15 596.557	4.965	–0.725	6.82E+07	A	Sc I	
15 597.163	5.410	–3.913	1.69E+08	A	Fe I	
15 597.326	6.726	–2.180	1.00E+05	A	Mg I	
15 598.870	6.240	–0.880	1.00E+05	A	Fe I	
15 598.890	4.690	–0.030	1.00E+05	A	Ti I	
15 599.134	4.690	–0.250	1.04E+08	A	Ti I	
15 599.210	5.948	–2.043	1.54E+08	2.50	Cr I	

Table 7. continued.

Wavelength [Å]	χ_{exc} [eV]	log gf	Γ_{rad} [rad s^{-1}]	van der Waal	Atomic/ionic species	New log gf values
15 599.346	4.475	–1.948	7.23E+07	A	Ti I	
15 600.208	4.684	–1.577	1.36E+08	A	Sc I	
15 600.500	5.011	–9.268	2.49E+08	A	Cr II	
15 600.972	5.228	–6.704	6.43E+07	A	Ca I	
15 601.810	5.229	–6.258	6.41E+07	A	Ca I	
15 601.839	5.773	–3.538	1.47E+08	A	Co I	
15 602.253	4.865	–1.550	1.25E+08	A	V I	
15 602.496	5.239	–3.253	5.14E+07	A	Cr I	
15 602.840	2.267	–1.70	2.31E+06	A	Ti I	*
15 603.753	6.727	–2.660	1.00E+05	A	Mg I	
15 603.882	5.303	–2.700	1.33E+08	A	Ni I	
15 604.220	6.240	0.49	1.00E+05	A	Fe I	*
15 605.073	2.345	–3.464	7.13E+07	A	Ti I	
15 605.680	5.300	–0.52	1.00E+05	A	Ni I	*
15 605.680	5.300	–1.010	1.00E+05	A	Ni I	
15 605.865	4.780	–5.161	1.58E+08	A	Ca I	
15 606.004	4.534	–1.544	3.45E+07	A	Sc I	
15 606.077	3.753	–3.902	2.50E+08	A	V II	
15 606.661	8.599	–2.301	5.86E+08	A	V II	
15 607.587	6.149	–2.192	1.15E+08	A	Mn I	
15 607.792	4.495	–8.994	3.05E+08	A	Fe II	
15 607.802	4.877	–3.048	8.93E+07	A	Ca I	
15 608.001	5.391	–8.875	2.71E+08	A	Mn II	
15 609.366	4.953	–0.336	7.00E+07	A	Sc I	
15 609.995	5.168	–3.409	9.62E+07	A	Ca I	
15 611.150	3.415	–3.12	1.57E+07	A	Fe I	*
15 611.219	6.019	–2.362	3.27E+08	A	Co I	
15 612.530	4.877	–2.568	8.91E+07	A	Ca I	
15 612.755	4.726	–4.292	5.89E+07	A	Mn I	
15 613.554	5.931	–2.090	1.05E+08	A	Fe I	
15 613.630	6.350	–0.210	1.00E+05	A	Fe I	
15 613.657	2.122	–3.503	5.66E+06	A	V I	
15 614.100	6.350	–0.42	1.00E+05	A	Fe I	*
15 614.345	5.931	–4.033	1.07E+08	A	Fe I	
15 614.442	4.798	–2.107	2.16E+08	A	Ti I	
15 615.047	2.505	–4.437	1.24E+08	A	V I	
15 615.071	4.057	–3.953	6.75E+07	A	V I	
15 617.601	7.113	–2.410	1.00E+05	1.30	Si I	
15 617.828	5.812	–4.036	2.64E+08	A	Cr I	
15 618.308	7.113	–2.630	1.00E+05	1.30	Si I	
15 619.265	5.458	–3.766	1.06E+08	A	Fe I	
15 619.958	2.294	–0.600	1.00E+05	A	Y I	
15 620.000	5.955	–2.692	3.06E+08	A	Co I	
15 620.610	5.002	–3.468	3.58E+08	A	Co I	
15 621.059	4.420	–1.755	2.18E+08	A	Ti I	
15 621.230	6.366	–3.375	2.42E+08	A	Ni I	
15 621.245	8.537	–4.000	1.00E+05	A	C I	
15 621.664	5.539	0.42	1.12E+08	A	Fe I	*
15 622.294	3.799	–2.606	2.45E+08	A	V II	
15 622.416	8.082	–0.595	5.19E+08	A	Ti II	
15 622.450	5.228	–5.071	5.81E+07	A	Ca I	
15 623.290	5.229	–3.535	5.79E+07	A	Ca I	
15 623.319	8.537	–3.160	1.00E+05	A	C I	
15 623.817	5.228	–3.510	5.81E+07	A	Ca I	
15 624.003	2.578	–4.991	1.61E+06	A	V I	
15 624.140	4.878	–2.342	8.89E+07	A	Ca I	
15 624.433	5.229	–2.483	5.79E+07	A	Ca I	
15 624.526	5.228	–2.765	5.81E+07	A	Ca I	
15 624.657	5.229	–2.614	5.81E+07	A	Ca I	
15 624.726	6.027	–0.428	8.51E+07	A	B I	
15 625.688	4.402	–2.193	2.24E+08	A	Ti I	
15 626.494	8.537	–2.970	1.00E+05	A	C I	
15 626.799	4.798	–1.400	2.17E+08	A	Ti I	
15 628.057	5.791	–3.081	2.16E+08	A	Mn I	
15 628.180	5.791	–4.060	1.87E+08	A	Co I	

Table 7. continued.

Wavelength [Å]	χ_{exc} [eV]	log gf	Γ_{rad} [rad s^{-1}]	van der Waal	Atomic/ionic species	New log gf values
15 628.448	1.950	–3.157	4.94E+06	A	V I	
15 629.081	6.027	–0.128	8.51E+07	A	B I	
15 629.370	5.946	–1.670	1.29E+08	A	Fe I	
15 629.384	5.946	–3.767	1.29E+08	A	Fe I	
15 629.630	4.559	–3.08	2.72E+08	A	Fe I	*
15 630.354	5.791	–3.259	2.15E+08	A	Mn I	
15 630.916	4.592	–1.275	1.85E+08	A	Sc I	
15 631.112	3.642	–4.10	8.04E+07	A	Fe I	*
15 631.430	4.777	–3.590	4.15E+07	A	Ti I	
15 631.476	7.125	–2.140	1.00E+05	A	Si I	
15 631.845	5.033	–2.109	5.58E+07	2.50	Sc I	
15 631.935	8.307	–4.217	4.97E+08	A	Fe II	
15 631.950	5.352	0.15	1.14E+08	A	Fe I	*
15 632.654	5.305	–0.01	9.71E+07	A	Ni I	*
15 633.079	5.045	–6.184	3.88E+07	A	Ca I	
15 633.996	4.073	–1.587	3.13E+08	A	V I	
15 634.730	6.054	–4.151	7.18E+07	2.50	Co I	
15 635.317	4.942	–2.073	1.36E+08	A	Sc I	
15 635.708	5.161	–2.323	1.18E+08	A	Ti I	
15 636.292	4.616	–8.153	3.08E+08	A	Fe II	
15 636.803	4.798	–2.010	2.17E+08	A	Ti I	
15 637.082	5.228	–7.521	1.87E+08	A	Ca I	
15 637.214	6.724	–2.763	4.50E+08	A	Fe II	
15 637.924	5.229	–6.571	1.87E+08	A	Ca I	
15 637.965	6.361	–2.20	2.33E+08	A	Fe I	*
15 638.029	5.507	–2.797	2.34E+08	A	Fe I	
15 638.300	6.076	–4.458	2.31E+08	A	Cr II	
15 638.472	6.734	–1.93	1.00E+05	A	Si I	*
15 638.919	5.814	–1.74	1.41E+08	A	Fe I	*
15 639.480	6.410	–0.88	1.00E+05	A	Fe I	*
15 640.869	6.212	–1.063	2.61E+08	A	Mn I	
15 640.872	6.098	–2.933	1.40E+08	A	Ni I	
15 641.002	5.539	–3.966	8.93E+07	A	Fe I	
15 641.701	1.931	–9.488	4.85E+06	A	V I	
15 641.922	5.494	–3.792	4.92E+08	A	Ni I	
15 642.338	5.303	–3.107	1.32E+08	A	Ni I	
15 643.072	6.317	–3.075	3.10E+08	A	V II	
15 643.219	8.548	–2.870	7.45E+08	A	V II	
15 643.380	6.783	–2.350	1.00E+05	A	Mg I	
15 645.010	6.310	–0.57	1.00E+05	A	Fe I	*
15 645.378	4.993	–1.720	8.71E+06	A	Al I	
15 645.415	7.113	–1.630	1.00E+05	1.30	Si I	
15 645.594	5.674	–3.812	1.00E+08	A	Co I	
15 645.843	7.166	–4.450	1.00E+05	A	Si I	
15 646.940	4.958	–3.147	3.43E+07	2.50	Sc I	
15 646.965	5.800	–2.066	1.24E+08	A	Cr I	
15 647.332	4.725	–3.269	1.72E+08	A	V I	
15 647.410	6.330	–1.05	1.00E+05	A	Fe I	*
15 647.479	4.059	–1.709	2.72E+08	A	V I	
15 648.535	5.426	–0.66	1.12E+08	A	Fe I	*
15 649.750	5.550	–3.027	3.24E+08	A	Fe I	
15 651.154	4.681	–3.859	1.80E+08	A	V I	
15 652.354	5.744	–2.363	3.12E+08	A	Co I	
15 652.870	6.250	–0.13	1.00E+05	A	Fe I	*
15 652.930	2.482	–9.038	4.40E+03	A	Fe I	
15 653.457	5.464	–4.076	8.04E+07	2.50	V I	
15 656.473	4.591	–3.391	1.10E+08	2.50	V I	
15 656.659	5.828	–2.847	1.26E+08	A	Fe I	
15 656.669	5.874	–1.80	1.41E+08	A	Fe I	*
15 659.317	5.537	–3.456	1.22E+08	A	Co I	
15 659.465	4.389	–2.263	1.83E+08	A	Cr I	
15 659.729	6.779	–4.050	1.00E+05	A	Mg I	
15 659.771	5.538	–3.001	2.97E+08	A	Fe I	
15 659.855	4.994	–1.420	8.71E+06	A	Al I	
15 660.259	6.779	–3.450	1.00E+05	A	Mg I	

Table 7. continued.

Wavelength [Å]	χ_{exc} [eV]	log gf	Γ_{rad} [rad s^{-1}]	van der Waal	Atomic/ionic species	New log gf values
15 660.375	6.779	–2.060	1.00E+05	A	Mg I	
15 661.290	5.607	–2.631	1.50E+08	A	Fe I	
15 661.555	4.506	–3.327	2.04E+08	A	Ti I	
15 661.611	4.795	–3.961	2.06E+08	A	Fe I	
15 661.655	4.650	0.266	8.83E+07	A	V I	
15 662.010	5.830	0.25	1.00E+05	A	Fe I	*
15 662.320	6.330	–0.80	1.00E+05	A	Fe I	*
15 662.686	4.850	–2.301	1.83E+08	A	Ti I	
15 662.826	3.087	–6.216	7.82E+06	A	Cr I	
15 663.047	5.140	–3.605	1.19E+08	A	Ti I	
15 663.905	5.102	–1.972	6.41E+07	2.50	Sc I	
15 664.735	4.370	–1.742	8.11E+07	A	Ti I	
15 665.240	5.980	–0.600	1.00E+05	A	Fe I	
15 665.994	5.233	–2.344	2.11E+08	A	Ti I	
15 666.299	4.411	–2.121	2.27E+08	A	Ti I	
15 666.679	5.520	–3.484	7.18E+07	A	Mn I	
15 666.728	3.096	–5.656	2.84E+03	A	Cr I	
15 667.956	4.888	–3.803	1.07E+08	A	Sc I	
15 670.130	6.200	–1.02	1.00E+05	A	Fe I	*
15 670.387	5.208	–5.097	3.73E+08	A	Co II	
15 670.977	4.953	–1.130	6.97E+07	A	Sc I	
15 671.000	6.330	–0.57	1.00E+05	A	Fe I	*
15 671.714	3.807	–1.851	3.16E+08	A	Sc I	
15 671.860	5.920	–1.40	1.00E+05	A	Fe I	*
15 672.156	5.611	–4.110	1.67E+08	A	Mn I	
15 672.574	5.941	–2.701	9.23E+07	2.50	Cr I	
15 673.150	6.250	–0.73	1.00E+05	A	Fe I	*
15 673.385	5.133	–0.57	6.68E+07	A	Mn I	*
15 673.982	5.883	–2.826	1.12E+08	A	Fe I	
15 674.122	6.022	–2.537	4.30E+08	A	Co I	
15 674.392	5.382	–3.351	1.45E+08	A	V I	
15 674.653	7.064	–1.30	1.00E+05	A	Si I	*
15 676.277	7.092	–4.110	1.00E+05	A	Si I	
15 676.599	5.106	–1.85	8.13E+07	A	Fe I	*
15 676.825	5.521	–2.786	1.25E+08	2.50	V I	
15 677.020	6.250	–0.730	1.00E+05	A	Fe I	
15 677.520	6.250	0.20	1.00E+05	A	Fe I	*
15 677.588	5.400	–2.641	1.26E+08	A	V I	
15 678.340	5.829	–2.030	2.16E+08	A	Fe I	
15 678.519	7.125	–2.40	1.00E+05	A	Si I	*
15 678.989	9.045	–3.905	8.30E+08	A	V II	
15 679.373	5.872	–3.699	1.15E+08	A	Fe I	
15 679.983	6.274	–3.160	1.00E+05	A	Si I	
15 680.081	4.697	0.10	2.04E+08	A	Cr I	*
15 680.194	5.094	–1.851	1.54E+08	A	Ti I	
15 680.863	5.297	–2.705	1.52E+08	A	Ti I	
15 681.658	2.851	–9.416	4.97E+04	A	Fe I	
15 682.020	5.410	–2.230	1.12E+08	A	Fe I	
15 682.510	6.370	–0.40	1.00E+05	A	Fe I	*
15 682.826	2.581	–4.766	1.61E+06	A	V I	
15 683.390	5.621	–1.970	1.47E+08	A	Fe I	
15 683.490	4.741	–2.909	1.46E+08	A	V I	
15 685.168	2.318	–5.865	1.72E+06	A	Ti I	
15 685.375	4.405	–2.849	2.24E+08	A	Ti I	
15 685.407	5.326	–3.206	1.27E+08	A	Ni I	
15 685.604	5.913	–2.700	1.20E+08	A	Fe I	
15 686.020	6.330	–0.20	1.00E+05	A	Fe I	*
15 686.165	5.913	–3.760	1.23E+08	A	Fe I	
15 686.222	4.664	0.430	8.99E+07	2.50	V I	
15 686.271	5.104	–3.404	6.43E+07	2.50	Sc I	
15 686.440	6.250	0.17	1.00E+05	A	Fe I	*
15 686.449	5.699	–3.009	3.63E+07	A	Cr I	
15 686.449	5.699	–3.118	3.52E+07	A	Cr I	
15 688.265	5.839	–4.013	1.20E+08	2.50	Co I	
15 689.225	4.650	–3.940	2.49E+08	A	V I	
15 691.850	6.250	0.61	1.00E+05	A	Fe I	*

Table 7. continued.

Wavelength [Å]	χ_{exc} [eV]	log gf	Γ_{rad} [rad s^{-1}]	van der Waal	Atomic/ionic species	New log gf values
15 692.750	5.385	–0.50	1.14E+08	A	Fe I	*
15 692.781	3.397	–5.402	1.50E+07	A	Fe I	
15 692.845	5.133	–0.827	6.89E+07	A	Mn I	
15 692.993	7.482	–0.980	4.47E+08	A	Sc II	
15 693.166	4.650	–4.064	2.42E+08	A	V I	
15 693.360	6.719	–1.20	1.00E+05	A	Mg I	*
15 693.360	6.719	–2.070	1.00E+05	A	Mg I	
15 693.360	6.719	–3.620	1.00E+05	A	Mg I	
15 693.454	6.719	–1.180	1.00E+05	A	Mg I	
15 693.454	6.719	–2.080	1.00E+05	A	Mg I	
15 693.555	6.719	–1.340	1.00E+05	A	Mg I	
15 693.782	5.497	–3.360	3.32E+08	A	Ni I	
15 693.929	5.161	–3.028	1.19E+08	A	Ti I	
15 694.500	6.240	–1.520	1.00E+05	A	Fe I	
15 694.964	5.219	–2.606	3.37E+08	A	Ti I	
15 696.319	2.616	–2.439	1.68E+06	A	V I	
15 696.371	4.396	–2.038	1.92E+08	A	Ti I	
15 696.472	5.156	–1.164	2.54E+08	A	Ti I	
15 696.911	5.538	–2.280	1.19E+08	A	Cr I	
15 698.508	5.519	–2.393	1.52E+08	A	Fe I	
15 698.765	5.476	–2.405	1.43E+08	A	Fe I	
15 698.979	1.887	–2.09	2.76E+06	A	Ti I	*
15 699.129	3.803	–3.855	2.45E+08	A	V II	
15 700.090	6.330	–1.180	1.00E+05	A	Fe I	
15 700.685	5.228	–7.463	1.86E+08	A	Ca I	
15 700.806	5.560	–3.905	9.62E+07	2.50	V I	
15 701.341	5.049	–7.810	7.66E+07	A	Ca I	
15 701.447	3.758	–2.916	2.50E+08	A	V II	
15 702.088	7.855	–3.000	3.59E+08	A	V II	
15 702.882	5.203	–2.348	2.64E+08	A	Ti I	
15 704.111	4.534	–2.852	3.28E+07	A	Sc I	
15 704.432	3.369	–2.618	4.05E+06	A	Cr I	
15 704.654	8.116	–1.903	4.76E+08	A	Ti II	
15 704.802	5.991	–3.081	3.40E+08	A	Co I	
15 705.312	5.049	–5.896	7.66E+07	A	Ca I	
15 706.183	5.330	–7.863	2.35E+08	A	Cr II	
15 707.047	4.958	–0.437	6.89E+07	A	Sc I	
15 708.380	4.196	–3.193	1.77E+07	A	Sc I	